Student-led experimental evolution reveals novel biofilm regulators of adaptation to multiple niches

AUTHORS

Abigail M. Matela[12], Colton W. Siatkowski[12], Changhua Yan[12], Sachin Thiagarajan[1], Vaughn S. Cooper[12]

[1]University of Pittsburgh School of Medicine, [2]Center for Evolutionary Biology and Medicine, Department of Microbiology and Molecular Genetics, Pittsburgh, PA, USA

ABSTRACT

We established a research-education partnership, EvolvingSTEM, that currently provides thousands of secondary school students the opportunity to conduct authentic research experiments centered on microbial evolution each year. Providing high school students access to research experiences not only improves learning and can have positive and long-lasting impacts on their attitudes towards science, but also gives them the opportunity to make impactful scientific contributions. Through EvolvingSTEM, students evolve populations of *Pseudomonas fluorescens* in a bead model that includes daily cycles of bacterial dispersal, attachment, and biofilm growth and observe heritable changes in colony morphology. Genome sequencing of 70 mutants that they picked identified parallel mutations in genes known to regulate biofilm growth (*wsp*, *yfiBNR*, *morA, fuzY*) and uncovered novel adaptations: loss-of-function mutations in phosphodiesterase PFLU0185 that did not alter colony morphology and mutations affecting periplasmic disulfide bond formation producing small colonies. PFLU0185 mutants rapidly and consistently reached high frequencies and phenotyping revealed roles in cyclic di-GMP regulation, biofilm formation, and motility, prompting us to name this gene *bmo* (biofilm and motility regulator). Competition experiments and microscopy demonstrated *bmo* mutants employ generalist strategies and coexist with their ancestor and specialist mutants through niche differentiation. Consequently, phenotypic diversity is maintained, with smooth (ancestral and *bmo*) colonies consistently outnumbering wrinkly and fuzzy variants. This study advances our understanding of biofilm genetic architecture while demonstrating that student-led research can uncover mechanisms of microbial adaptation relevant to *Pseudomonas* infection biology.

IMPORTANCE

Bacterial biofilms dominate microbial life, yet their evolutionary genetics remain incompletely understood. Extensive replication of experiments that employ similar, but not identical, biofilm selection models can provide valuable insights into mechanisms of adaptation. We demonstrate that this can be achieved through university-education partnerships that engage secondary school students in authentic research. Student-led experiments revealed that loss-of-function mutations in a conserved phosphodiesterase, PFLU0185/*bmo*, dominate evolved populations without changing colony morphology. This finding, combined with diverse, less frequent mutants that alter colony morphology informs the process of biofilm niche differentiation. This work also demonstrates the power of distributed research networks for discovering new genetic pathways of adaptation. Students gained authentic research experience, potentially inspiring them to become scientists, while identifying mutants adapted to discrete conditions that maintain diversity within biofilms. This synergy between education and discovery offers a scalable model for addressing complex biological questions while developing scientific literacy in diverse classrooms.

INTRODUCTION

Despite being the dominant form of microbial life, our understanding of the ecology, evolution, and genetic controls of adaptation within biofilms is still developing. What we and many others have learned is that bacteria evolve rapidly and conspicuously, often by producing new colony morphologies, when selected to improve surface growth in experimental models as well as in clinical and environmental settings (Stewart & Franklin, 2008; Poltak & Cooper, 2011; Traverse et al., 2013; Ellis et al., 2015; Nadell et al., 2016). This dynamic can be captured in simple experiments conducted by secondary school students that not only improves their learning experiences but also provides them the opportunity to contribute to cutting-edge scientific research (Cooper et al., 2019; Spiers, 2014; Taylor et al., 2024).

We might expect that interactions in biofilms would be complex as cells engineer their environment by secreting polymers that bind them to a surface and protect them from stresses, competitors, or predators. Two overlapping processes can explain the origin and maintenance of phenotypic diversity within biofilms. The first is environmental structure itself, which allows multiple phenotypically equivalent mutants to arise and coexist in different regions (Kassen & Rainey, 2004). The second is ecological interactions made possible by structure, for example, when an early adhering population facilitates the attachment of different types (Habets et al., 2006; Harris et al., 2021). However, the genetic and phenotypic outcomes of these processes are less clear but broadly important in natural and engineered systems, such as wastewater treatment (Røder et al., 2016) and in the clinic (Trubenová et al., 2022). For example, high-biofilm forming bacterial and fungal mutants often arise during chronic infections, are associated with increased resistance to antibiotics and immune phagocytes, and worsen patient outcomes (Hall-Stoodley et al., 2004; Flemming & Wuertz, 2019; Pestrak et al., 2018). There is a need to broadly characterize the spectrum of genotypes and phenotypes that generate biofilm diversity. Experimental evolution of microbial populations under conditions favoring biofilm combined with contemporary genomic analysis can be a powerful screen of these traits.

Our laboratory previously developed an *in vitro* model to study evolution throughout the entire biofilm life cycle of surface attachment, biofilm assembly, dispersal, and re-colonization (Poltak & Cooper, 2011). In short, bacteria are cultured in test tubes that contain growth media and a polystyrene bead, which serves as a surface for bacteria to colonize and form a biofilm.

82 The biofilm-covered bead is then transferred to a new test tube with fresh media and a sterile
83 bead. Beads are serially transferred to select for biofilm-adapted mutants that can disperse from
84 the old bead and recolonize and assemble a new biofilm on the new bead every 24 hours. This
85 model has been used by us to better understand the dynamics of biofilm evolution and
86 associated ecological diversification in multiple species (*Burkholderia cenocepacia*,
87 *Acinetobacter baumannii*, *Pseudomonas aeruginosa*) under various environmental stressors
88 (e.g., nutrients, antibiotics) (Poltak & Cooper, 2011; Traverse et al., 2013; Cooper et al., 2014;
89 Ellis et al., 2015; O'Rourke et al., 2015; Flynn et al., 2016; Turner et al., 2018; Santos-Lopez et
90 al., 2019; Scribner et al., 2020; Mhatre et al., 2020; Harris et al., 2021). The bead model has
91 also been adapted by many others to address similar questions and is routinely paired with
92 whole genome sequencing of mutant clones and evolved populations to identify causes of new
93 phenotypes (Henriksen et al., 2022; Oakley et al., 2021; Trampari et al., 2021). A surprising
94 finding from these studies is the extent of genetic parallelism rather than a diverse array of
95 pathways to adaptation. Despite the intuition that the biofilm life cycle is both structured and
96 heterogeneous, and the observation of various colony phenotypes, mutations in relatively few
97 genes encoding major biofilm regulators accounted for most of the adaptations (Mhatre et al.,
98 2020; Santos-Lopez et al., 2019).
99
100 One possible explanation for convergent evolution in the biofilm bead model is that each
101 study was conducted by one or few investigators using well controlled conditions, thereby
102 focusing selection on limited traits. Higher experimental replication by many different
103 researchers could address this concern. For this reason and many others related to improving
104 learning and access to authentic research, we adapted the bead model for use in secondary
105 school classrooms (Cooper et al., 2019). In this research-education partnership, students work
106 with the harmless plant probiotic bacterium, *Pseudomonas fluorescens* strain SBW25, which is
107 both a model of this environmentally relevant species and shares many orthologs with the
108 opportunistic pathogen *P. aeruginosa*. This program is called EvolvingSTEM and now engages
109 thousands of students a year in authentic microbiology research in grades 6-12 in more than 20
110 schools in several U.S. states. Previous research on *P. fluorescens* SBW25 identified biofilm-
111 related adaptations to static culture conditions, where populations rapidly evolve to form a
112 biofilm mat at the oxygen-rich, air-liquid interface (Koza et al., 2017). The evolved populations
113 diversified into three distinct colony morphologies: (1) smooth and round (the ancestral

114 phenotype), (2) wrinkly, and (3) fuzzy (Rainey & Travisano, 1998). It is this rapid evolution to
115 produce pellicles that encouraged us to use *P. fluorescens* with our bead model to study its
116 adaptation to biofilm growth with students.
117
118 The most conspicuous new colony morphology seen in previous experiments is the
119 wrinkly phenotype. This phenotype commonly results from mutations in one of three genetic
120 pathways – *wsp*, *yfiBNR* (or *aws*), and *morA* (or *mws*) – that regulate the production of a
121 secondary messenger, bis-(3'-5')-cyclic dimeric guanosine monophosphate (cyclic di-GMP)
122 (McDonald et al., 2009). Cyclic di-GMP controls biofilm formation by regulating the activity of
123 several downstream genes and proteins (Jenal et al., 2017). The production of cyclic di-GMP is
124 regulated by the opposing activity of two enzyme families: diguanylate cyclases (DGCs) that
125 synthesize cyclic di-GMP and phosphodiesterases (PDEs) that degrade it (Jenal et al., 2017).
126 High cellular levels of cyclic di-GMP are associated with surface attachment and biofilm
127 production, while low levels are associated with increased motility, solitary behavior, and
128 bacterial dispersal (Laventie, Benoit-Joseph, 2020). Mutations in the *wsp*, *yfiBNR*, and *morA*
129 pathways lead to constitutive activation of a DGC, which results in overproduction of cyclic di-
130 GMP (Malone et al., 2007; McDonald et al., 2009), and, ultimately, increased biofilm formation
131 through increased production of acetylated cellulose (Spiers et al., 2002, 2003). In contrast,
132 fuzzy phenotypes are a result of mutations in *fuzY*, which encodes a β-glycosyltransferase
133 predicted to modify LPS O-antigens. Mutations in *fuzY* are thought to promote cell-cell contact
134 but the mechanistic benefit of mutations in this gene are less well understood (Ferguson et al.,
135 2013).
136
137 *P. fluorescens* populations evolved by high school students with our EvolvingSTEM
138 evolution-in-action experiment often exhibit diverse colony morphologies within and among
139 populations that resemble those seen under selection in static culture conditions (Cooper et al.,
140 2019). We wondered if the phenotypic similarities of mutants adapted to static culture and those
141 in our bead model are caused by the same underlying genetic changes, so we sequenced 70
142 clones from populations almost entirely evolved by high school students. We found that *P.*
143 *fluorescens* adapts to form biofilms on surfaces through mutations in some of the same genetic
144 pathways as those used to form pellicles in unshaken vials and also uncovered novel biofilm
145 adaptations. We then sought to identify what drives evolutionary dynamics in our bead model

146 and whether these dynamics differ when bacteria are grown in subinhibitory levels of the
147 common antimicrobial triclosan, which was used to prevent fungal and bacterial contamination
148 at some schools. This led to the discovery that biofilm adaptation in our model is primarily driven
149 by lineages that do not change colony appearance but acquire loss-of-function mutations in
150 PFLU0185, a highly conserved gene across pseudomonads encoding a DGC and dominant
151 PDE (Cai et al., 2022, 2022; Eilers et al., 2022; Eilers, Yam, et al., 2024; Wei et al., 2019).
152 Although PFLU0185 mutants share the same colony morphology as their ancestor, further
153 phenotyping revealed adaptations in biofilm formation and motility. We therefore suggest
154 renaming this locus *bmo*, for biofilm and motility regulator. Population sequencing, microscopy,
155 and multi-genotype competition experiments suggest that *bmo* mutants coexisted with their
156 ancestor and with rarer, genetically diverse lineages producing wrinkly and fuzzy colonies in
157 dynamics that can be explained by multi-niche selection (Brisson, 2018).
158
159 **RESULTS**
160
161 **Student-led experiments rapidly uncover diverse phenotypes**
162 Our EvolvingSTEM evolution-in-action experiment allows students to observe bacterial
163 populations evolving and diversifying within days as they adapt to a daily selection regime to
164 complete the entire biofilm life cycle of dispersal, surface attachment, and biofilm maturation.
165 Students work with a harmless plant probiotic bacterium, *P. fluorescens* strain SBW25. As the
166 populations evolve, students can observe at least two types of phenotypic change. First, as high
167 biofilm-forming mutants increase in frequency in the population, students often see a more
168 robust layer of biofilm form in their test tubes at the air-liquid interface. Second, students can
169 observe changes in the colony morphologies of bacteria grown on agar plates. While the
170 ancestral population produces only smooth, circular colonies, evolved populations often exhibit
171 diverse, conspicuous colony morphologies within and among populations (Fig. 1).
172
173 Students from three high schools – Winnacunnet High School (WHS, Hampton, NH,
174 N=~250), Pittsburgh Science and Technology Academy (Pittsburgh, PA, N=25), and Allderdice
175 High School (Pittsburgh, PA, N=24) – conducted experiments under slightly different conditions.
176 Changes to the experimental protocol were made to accommodate class requirements and
177 increase the accessibility of EvolvingSTEM in varied classroom settings (our updated protocol

178 can be found in supplemental materials). While WHS used standard aseptic technique, in other
179 schools, we added the commonly used antimicrobial compound triclosan to the media and agar
180 plates to broadly inhibit bacterial and fungal contamination. *Pseudomonas* species are known to
181 tolerate or resist triclosan (Schweizer, 2001; McFarland et al., 2021), and this eliminates the
182 need to use a flame in schools that do not have access to Bunsen burners and/or do not feel
183 comfortable having students work near an open flame. Another difference was that WHS
184 aerated growing bacterial cultures on a roller drum, which was not available in most classrooms,
185 so we switched to using orbital shakers to aerate growing cultures.
186
187 Students plated samples of their bead-attached bacterial populations on agar at the
188 beginning and end of the experiment. Ancestral *P. fluorescens* clones produce only smooth,
189 round colonies, and this was the only morphology identified on the early plating day. Most bead-
190 adapted populations contained wrinkly colony variants on the final plating day, and some had
191 fuzzy and small colony variants (Fig. 1). Wrinkly and fuzzy colony variants had a similar
192 appearance to those identified when *P. fluorescens* is under selection for the formation of
193 biofilm mats in static culture conditions (Koza et al., 2017). While our experimental design also
194 selects for biofilm-adapted mutants, it differs from static selection experiments in that bacteria
195 must colonize a new surface each day, completing the entire biofilm life cycle of dispersal,
196 attachment, biofilm assembly, and matrix building. We therefore explored if the convergent
197 colony phenotypes we identified in these experiments was the result of convergent mutational
198 targets by sequencing the genomes of wrinkly and fuzzy clones from independent populations.
199 In addition, we sequenced the genomes of smooth colonies, which were identical in appearance
200 to the ancestor, and small colony variants, which were the only other unique morphology noted
201 in these experiments (Fig. 1).
202
203 **Biofilm adaptations include mutations affecting cyclic di-GMP production, LPS O-antigen**
204 **structure, and periplasmic protein folding**
205 Two remarkable properties of this collection of mutant genomes deserve highlighting
206 before we explore the genes affected or their functional implications. First, in 55 of 70 mutants,
207 only one mutation was identified, meaning that this single mutation experienced strong selection
208 to rise to a detectable frequency and, in most cases, change the colony morphology (Table 1,
209 Table S1). Consequently, the biofilm bead model serves as a potent forward genetic screen for

210 single mutations that influence biofilm-related fitness. Of the remaining 15 mutants, 13 had two
211 mutations and one had three mutations. Second, the extent of site-specific parallelism in these
212 mutants is extraordinary: 13 individual mutations occurred more than once in different clones.
213 Although it is possible that a few instances of parallel mutations were not entirely independent,
214 e.g. from the same school and year, most clearly arose independently from different schools
215 and years. Exceptional examples include one SNP in *wspF* that was observed in six clones and
216 another 33bp deletion in *yfiR* observed five separate times (Table 1). This observation suggests
217 extremely strong selection for certain mutations, a locally higher mutation rate, or both. Overall,
218 23 unique genes became mutated and were affected by a roughly equal mix of small
219 insertion/deletions (indels) and SNPs with fewer larger deletions. This spectrum of mutations
220 demonstrates that *P. fluorescens* experiences strong selection for a narrow set of traits in the
221 biofilm bead model that often favors identical mutations in independent experiments.
222
223 The genomes of 57 clones with wrinkly phenotypes were sequenced from 50
224 independently evolved biofilm populations. In agreement with previous studies on biofilm
225 formation in static culture conditions, causative mutations were identified in the *wsp*, *yfiBNR*,
226 and *morA* pathways (Fig. 2, Table 1), which supports a critical role for these pathways in biofilm
227 regulation under diverse selective regimes. Mutations in the *wsp* pathway were the most
228 common cause of wrinkly phenotypes across all sequenced clones, with approximately 70%
229 having a single causative mutation in this pathway. Mutations were primarily found in *wspF*
230 (PFLU1224, 33 clones), followed by *wspA* (PFLU1219, 6 clones). In addition, a single clone had
231 a 335 base-pair deletion that overlapped the coding regions of *wspC* (PFLU1221) and *wspD*
232 (PFLU1222), resulting in a WspC-WspD fusion protein. The *yfiBNR* pathway was the second
233 most common cause of wrinkly phenotypes, with approximately 16% of clones having a single
234 causative mutation in *yfiR* (PFLU5211, 9 clones). Mutations in *morA* (PFLU5329, 5 clones) were
235 the least common cause of wrinkly phenotypes, with approximately 9% of clones having a single
236 causative mutation. Surprisingly, all three clones isolated at Allderdice had mutations in two
237 pathways. These clones contained a single, nonsynonymous SNP in the PDE domain of *morA*.
238 One clone had an additional nonsense mutation in *wspF*; one had an additional missense
239 mutation in *wspA*; and one had an additional deletion in the linker region between the DGC and
240 PDE domains of *morA*. These mutants indicate that the sequential acquisition of multiple
241 mutations in pathways influencing cyclic-di-GMP metabolism can be beneficial.

242

243 Fuzzy mutants were identified in evolved populations at several schools, although less
244 frequently than wrinkly mutants. While we did not sequence any fuzzy mutants from high school
245 experiments, two fuzzy mutants isolated in the laboratory had predicted loss-of-function
246 mutations in *fuzY* (PFLU0478) (Fig. 3). In addition, we sequenced the genomes of five small
247 colony variants isolated by students and in the laboratory. These mutants contained single
248 mutations in a predicted two-component system sensor histidine kinase, *dsbS* (PFLU4380), or
249 in the operon it is predicted to regulate, *dsbD* (PFLU4382)-*dsbG* (PFLU4384) (Fig. 3). Three
250 clones had an in-frame deletion in the N-terminal region of *dsbS*, one clone had a 110 base-pair
251 deletion that overlapped the coding regions of *dsbE* (PFLU4383) and *dsbG*, resulting in a DsbE-
252 DsbG fusion protein, and one clone had a mutation in the intergenic region upstream of *dsbR*
253 (PFLU4381) and *dsbD* (Fig. 3). Lastly, we also sequenced clones from five evolved populations
254 that retained the ancestral smooth morphology. Although one smooth clone had no mutations,
255 four clones had a mutation in a gene encoding both DGC and PDE domains, PFLU0185, and
256 this was the only mutation identified in three clones (Fig. 3). We have named this gene *bmo* for
257 its roles in biofilm formation and motility, which are further described below.

258

259 **Strong selection for mutations in *bmo* during adaptation to the experimental biofilm life**
260 **cycle**

261 We were intrigued by the discovery of mutations in a DGC-PDE encoding gene that did
262 not change the mutant colony phenotype. Although an objective of the EvolvingSTEM program
263 is to visually demonstrate adaptation by natural selection by observing novel colony phenotypes
264 after selection for improved biofilm formation, in fact, most populations have a majority of
265 colonies that retain the smooth appearance of the ancestor after one week of passage. This
266 suggests that focusing only on colony variants may miss biofilm adaptations. To address this
267 limitation, we conducted a 15-day evolution experiment in which we used whole-population,
268 whole-genome sequencing to identify all mutations reaching appreciable frequency in biofilm
269 populations regardless of whether they alter colony appearance. We also replicated this
270 comparison in media containing triclosan, which we use in classrooms to guard against
271 contamination and which appears to accelerate rates of diversification. Specifically, four
272 replicate biofilm populations were propagated with and without 25μg/mL triclosan for 15 days.
273 We plated the bead-attached portion of each population after 4, 8, 11, and 14 transfers to

274 observe phenotypic changes to population colony morphologies over time and performed
275 whole-population, whole-genome sequencing after 2 and 14 transfers (Table S2, Fig. 4). We
276 noted three distinct colony morphologies, wrinkly, fuzzy, and small, in addition to the ancestral,
277 smooth phenotype. Populations grown in triclosan had moderately increased diversity on the
278 earliest plating day, but this diversity decreased over the course of the experiment, with all
279 populations having over 95% smooth colonies by the final plating. Populations that were grown
280 without triclosan maintained slightly higher diversity over time, and all populations had between
281 90-95% smooth colonies by the final plating (Fig. 4).
282
283 Surprisingly, mutations in the *bmo* locus were the only gene-level parallel genetic
284 change in all biofilm populations, and they rose to detectable frequencies by the third day of the
285 experiment in media containing triclosan, but not in media without triclosan (Fig. 4, Table S2).
286 Multiple independent mutations in *bmo* were present within each of the three biofilm populations
287 with added triclosan at day 3 at 16.7%, 42.3%, and 50% cumulative frequency, and by day 15
288 all eight biofilm-adapted populations had *bmo* mutants at >16% cumulative frequency. The only
289 other notable biofilm-related mutation that we observed was in *fuzY*, which reached a frequency
290 of 11.2% in one population that was grown without triclosan. Furthermore, three of the four
291 populations grown with added triclosan gained mutations in a transcription factor, *anr*
292 (PFLU4570), and one of the genes it regulates, *hemN* (PFLU4568). These mutations may be
293 adaptations to growth in triclosan and will be the subject of future study.
294
295 **Mutants are differentiated in biofilm phenotypes including attachment, assembly, and**
296 **motility**
297 We predicted that mutations in *bmo* achieved the highest frequencies and repeatedly
298 evolved in our biofilm selection model because they are best adapted to the cyclical
299 requirements to attach to the plastic bead, assemble biofilms, and then disperse to colonize a
300 new bead. We therefore characterized the motility, biofilm production, and cyclic di-GMP
301 production for a representative *bmo* loss-of-function mutant with a single nucleotide insertion
302 that results in a premature stop codon truncating both the DGC and PDE domains (Table 1). We
303 compared its biofilm associated phenotypes to a representative wrinkly (*wspF* Q185*) and fuzzy
304 (*fuzY* Q11*) mutant, along with the *P. fluorescens* SBW25 ancestor from which these mutants
305 evolved.

306

307 We first compared three common types of bacterial motility – swarming, swimming, and
308 twitching. All biofilm-adapted mutants had reduced swarming and swimming motility in
309 comparison to the ancestor (Fig. 5A, 5B). *wspF* mutants were the least motile, while *fuzY* and
310 *bmo* mutants had intermediate phenotypes. Twitching motility was not displayed by any biofilm-
311 adapted mutants or the ancestor, confirmed by comparison to *Pseudomonas aeruginosa* PAO1
312 which possesses twitching motility (Fig. S1).

313

314 To estimate biofilm production by each mutant, we adapted the traditional crystal violet
315 96-well plate assay (O'Toole & Kolter, 1998) to better align with how bacteria form biofilms in
316 our bead model. Bacteria were cultured for 24 hours in test tubes containing media and two
317 plastic beads. We quantified total biofilm production by staining one bead with crystal violet,
318 removing excess stain by washing the bead in water, and solubilizing biofilm-bound crystal
319 violet by vortexing the bead in solvent. We quantified biofilm population size by vortexing and
320 dilution-plating from the second bead. When grown in QB medium, *bmo* and *wspF* mutants
321 have the highest total biofilm production and population size (Fig. 5C, 5D). One caveat to note is
322 that *wspF* mutant populations often acquire compensatory, suppressor mutations that can rise
323 to high frequencies in overnight cultures, so between 20%-40% of the colonies counted had a
324 smooth, ancestral phenotype. When grown in media with added triclosan, total biofilm
325 production is doubled in *bmo*, *fuzY*, and the ancestor and quadrupled in *wspF* (Fig. 5C, 5D).
326 Moreover, the population size of all genotypes is less than half that observed in triclosan-free
327 media (Fig. 5C, 5D). Planktonic growth is also slower when triclosan is included in the media
328 and final population sizes are smaller (Fig. S2).

329

330 To determine how these biofilm-adapted mutations affect cyclic di-GMP metabolism, we
331 used a GFP reporter plasmid that responds to the intracellular concentration of cyclic di-GMP to
332 estimate these changes. Levels of cyclic di-GMP differed significantly among *P. fluorescens*
333 mutants following 24 hours of growth in QB media (Fig. 5E). Cyclic di-GMP concentrations were
334 highest for *bmo* and *wspF* mutants, with *wspF* producing nearly double the amount of cyclic di-
335 GMP as *bmo*. Surprisingly, the *fuzY* mutant produced approximately half as much cyclic di-GMP
336 as the ancestor, although this gene is not reported to have a role in the regulation of cyclic di-
337 GMP. Taken together, these results demonstrate that *bmo* regulates biofilm formation and

338 motility and loss-of-function mutations in this gene allow for the optimization of biofilm
339 production and planktonic growth in our bead model.
340
341 We sought to understand how the different macroscopic and regulatory phenotypes of *P.*
342 *fluorescens* mutants generated distinct microscopic biofilm phenotypes. We therefore used
343 confocal microscopy to image biofilms produced by our representative *bmo*, *wspF*, and *fuzY*
344 mutants as well as the ancestor that contained a constitutively active fluorescent reporter
345 inserted at a neutral site on the chromosome. Both the ancestor and *bmo* formed relatively
346 confluent biofilms of even thickness and their similar appearances suggest that they would
347 compete for the same niche space on the bead (Fig. 6). In contrast, the *fuzY* biofilm was more
348 clumped and uneven in thickness and coverage, whereas the *wspF* biofilm was surprisingly
349 sparse, with small, dense clusters (Fig. 6). It is notable that we imaged biofilms on glass slides
350 rather than on the polystyrene beads on which these mutants evolved, and that the supernatant
351 of the *wspF* cultures contained large aggregates that did not adhere well to glass. To explore
352 how these mutants interact in a diverse biofilm, we imaged mutants with different fluorescent
353 markers that were co-cocultured in pairs (Fig. S3). Overall, the observed patterns of biofilm
354 assembly agreed with predictions from mutant growth alone, with interspersed and confluent
355 growth by *bmo* and the ancestor but fewer discrete patches of different sizes and forms
356 produced by *wspF* and *fuzY.* Taken together, these images indicate that biofilm mutants in
357 different pathways are ecologically distinct and produce clusters or coatings of varying biomass
358 and form, both alone and in mixture.
359
360 **Genetic diversity during biofilm selection is maintained by competition and niche**
361 **differentiation**
362 An important and unusual finding from these studies is that *P. fluorescens* populations
363 grown in the biofilm bead model rapidly and repeatedly diversify into multiple phenotypes and
364 genotypes that coexist, with no genotype ever reaching 100%. This observation implies that
365 selection acts strongly on mutants that inhabit different niches of varied capacity. This leads to
366 the prediction that if putative niche specialists are mixed in equal amounts and propagated, their
367 frequencies should equilibrate according to the capacity of each niche and the relative
368 competitiveness of each mutant in conditions of niche overlap (e.g., growth on a common
369 carbon source). We created a mixed population of the three, representative biofilm-adapted

370 mutants *bmo*, *wspF*, and *fuzY* and their *lac*-marked ancestor. We used this mixed population to
371 inoculate six replicate cultures grown in our bead model of biofilm growth for four days without
372 triclosan and plated daily to determine the frequency of each genotype on newly colonized
373 beads (Fig. 7). As predicted, all genotypes coexisted within each population, with *wspF* and
374 *fuzY* mutants generally at low frequencies and the *bmo* mutant and ancestor at intermediate
375 frequencies. In addition, frequencies of *bmo* and WT were anticorrelated in half of the replicates,
376 which suggests they occupy differentiated but overlapping niches, as the microscopy indicated
377 and ecological literature supports (Fig. 6) (Caplat et al., 2008; Chesson, 2000). We used linear
378 regression to test this hypothesis for all genotype combinations and found a significant, negative
379 relationship for the *bmo* mutant frequency with frequencies of all other genotypes, which is
380 consistent with competition (Table 2, Fig. S4). In summary, our model of the biofilm life cycle
381 exerts strong, parallel selection for different phenotypes that balance biofilm production, growth,
382 dispersal, and reattachment in different ways. Mutants adapted to different aspects of these
383 traits can coexist by invading in conditions in which they are more fit, while declining in
384 conditions where they are less competitive.
385
386 **DISCUSSION**
387
388 **Student experiments discover new genetic pathways of adaptation to the biofilm life**
389 **cycle**
390 Involving secondary school students in distributed scientific experiments in their own
391 science classrooms offers complementary promises, including: 1) a high level of replication that
392 can broadly test a common hypothesis, and 2) developing a community of teachers and
393 learners who are connected by a common set of research skills, experiences and findings.
394 Here, we not only report evidence that both promises can be met, but also that students
395 contributed to expanding our knowledge of the genetics of adaptation to the biofilm life cycle.
396 Their experiments with the biofilm bead model selected for phenotypes that excel during daily
397 cycles of dispersal, recolonization, and biofilm assembly. By picking many representative clones
398 with these phenotypes and then genotyping them by whole-genome sequencing, we use
399 experimental evolution as a powerful forward genetic screen. This approach identified mutants
400 that support previous findings from pellicle selection experiments and also uncovered novel
401 adaptive pathways within the biofilm lifestyle. These findings support the hypothesis that biofilm

402 selection acts on traits governed by a few central regulators, leading to strong parallel evolution
403 across experiments. They also reveal that different selective environments, for example
404 associated with varied implementation in classrooms, can uncover alternative adaptations in
405 novel pathways to biofilm formation. Because most of these mutants contain only one mutation
406 in their genome, the relationships between genotype and phenotype are direct. In this section,
407 we discuss predicted molecular and biochemical effects of these mutants in detail, several of
408 which strengthen or modify existing models of *Pseudomonas* biofilm gene regulation. We begin
409 by analyzing mutations producing the well-known wrinkly and fuzzy colony morphologies and
410 follow with discussion of the potential causes of beneficial small colony variants.
411

412 **Student-selected colony variants support previous findings of genetic pathways**
413 **important for biofilm formation**

414 The most common cause of wrinkly phenotypes was mutations in the *wsp* pathway, a
415 chemotaxis-like system composed of 7 genes: *wspA-R*, under the control of a single promoter
416 (Fig. 2) (Bantinaki et al., 2007). WspA is a methyl-accepting chemotaxis protein that is anchored
417 at the cytoplasmic membrane by the scaffolding proteins WspB and WspD. Upon sensing an
418 environmental signal, conformational changes in the WspA-B-D complex result in WspA being
419 methylated by WspC, a constitutively active methyltransferase. This begins a signaling cascade
420 that activates WspE, a histidine kinase response regulator. WspE goes on to activate WspR, a
421 DGC, through phosphorylation, increasing levels of cyclic di-GMP and ultimately leading to
422 increased biofilm formation through increased cellulose production (Spiers et al., 2002, 2003).
423 WspE also phosphorylates WspF, a methylesterase that negatively regulates the system by
424 demethylating WspA. In general, the Wsp pathway mutations we identified are predicted to
425 cause constitutive production of cyclic di-GMP and, consequently, increased biofilm formation.
426 We identified deletions in *wspA* that have been shown *in P. aeruginosa* to lock the pathway on
427 in a methylation-independent manner (A. Xu et al., 2021), whereas nonsynonymous mutations
428 in the *wspA* signaling domain likely disrupt the stability of its trimer-of-dimer interactions,
429 increasing WspE activation (O'Connor et al., 2012; Kessler et al., 2021). The mutation
430 producing a WspC-WspD fusion protein likely leads to hypermethylation of WspA because it
431 physically links WspC to the WspA-B-D complex (Kessler & Kim, 2022). The many different
432 mutations in *wspF* include nonsynonymous substitutions, many of which occurred at the same
433 site repeatedly, insertions, and deletions, including frameshift and nonsense mutations that

434 introduced premature stop codons (Fig. 2). These mutations almost certainly interfere with
435 WspF activation and/or its ability to demethylate WspA (O'Neal et al., 2022; A. Xu et al., 2021).
436
437 The second most common cause of wrinkly phenotypes were mutations in the *yfiBNR*
438 pathway, which is composed of three genes under the control of a single promoter (Fig. 2). YfiN
439 is a DGC that is localized to the cytoplasmic membrane and negatively regulated by the
440 attachment of the periplasmic YfiR protein (Malone et al., 2010, 2012). In response to
441 membrane stress, YfiB, a lipoprotein located at the outer membrane (Malone et al., 2012),
442 adopts an elongated conformation, which allows it to bind to and sequester YfiR (Li et al., 2018;
443 M. Xu et al., 2016). YfiN is therefore released from its negative regulation and able to catalyze
444 cyclic di-GMP production, promoting biofilm formation (Fig. 2). The C-terminal region of *P.*
445 *aeruginosa* YfiR is predicted to contain the attachment site to YfiN (Malone et al., 2012; Yang et
446 al., 2015); therefore, the *yfiR* missense and nonsense mutations we discovered in this region
447 may eliminate YfiR's ability to bind to YfiN. *P. aeruginosa* YfiR forms a dimer in its active form
448 via salt bridges formed by R98 and D80 and hydrogen bonds between T76 (Yang et al., 2015).
449 Notably, five *yfiR* mutants experienced the same 33bp deletion from T75 to T85 in *P.*
450 *fluorescens* that removes these homologous regions involved in dimerization. In addition, both
451 this deleted region and the downstream 33bp deletion contain or are located close to conserved
452 cysteine residues that in *P. aeruginosa* form disulfide bonds important for proper protein folding
453 (Yang et al., 2015). Deletions in these regions are therefore likely to lead to protein misfolding
454 that inhibits YfiR's ability to bind YfiN, thereby derepressing the DGC which promotes a biofilm
455 lifestyle.
456
457 Mutations in *morA* were the third most likely cause of wrinkly phenotypes. MorA is a
458 single protein localized to the cytoplasmic membrane that contains two PAS sensor domains as
459 well as active DGC and PDE domains, so it can catalyze both production and degradation of
460 cyclic di-GMP (Fig. 2) (McDonald et al., 2009; Phippen et al., 2014). We identified two identical
461 nonsynonymous substitutions in the DGC, three mutations affecting the linker region between
462 DGC and PDE domains that likely cause conformational changes that increase DGC activity
463 (Mhatre et al., 2020), and three identical mutations in the PDE that appear to disrupt its activity
464 (Fig. 2). The elevated biofilm of all these mutants indicates that their effects increase cyclic di-
465 GMP levels.

466

467 Fuzzy colony phenotypes are caused by loss-of-function mutations in *fuzY* (Fig. 3). In *P.*
468 *fluorescens* SBW25, *fuzY* is part of a five-gene operon that was predicted to encode a β-
469 glycosyltransferase that plays a role in modifying lipopolysaccharides (LPS) O-antigens, the
470 outermost portion of the LPS (Ferguson et al., 2013). The reciprocal best match of *fuzY*
471 homologs in *P. aeruginosa* strain PAO1 is *wapH*, which participates in synthesis of the LPS core
472 (Lam et al., 2011). In either case, in addition to roles in pathogenesis and symbiosis, O-antigen
473 structure plays an important role in bacterial adhesion and cohesion (Lerouge & Vanderleyden,
474 2002). In *P. aeruginosa*, O-antigen mutants exhibit increased cell-cell cohesion and increased
475 adhesion to glass surfaces (Lau et al., 2009). In our bead selection experiment, we expect that
476 mutations in *fuzY* are beneficial because they increase both cell-cell and cell-surface contact,
477 which would provide an advantage in adhering to the surface of the bead.
478

479 **Student findings uncover new pathways to biofilm adaptation predicted to disrupt**
480 **periplasmic protein folding**

481 Biofilm evolution experiments with our bead model often select for small colony variants
482 with increased Congo Red binding, which is consistent with higher cellulose production (Fig. 1;
483 Fig. S5). These phenotypes were consistently caused by mutations in a pathway that regulates
484 the formation of disulfide bonds, *dsbRS* and *dsbDEG*, which is critical for some proteins to be
485 properly folded into their active state conformation (Fig. 3). Most knowledge of enzymes
486 involved in the formation of disulfide bonds comes from studies in *Escherichia coli* (J. C. A.
487 Bardwell et al., 1991; J. C. Bardwell et al., 1993). In *E. coli*, the periplasmic oxidoreductase
488 DsbA catalyzes formation of disulfide bonds but is thought to perform this reaction
489 indiscriminately by introducing bonds between neighboring cysteines (Bader et al., 2000; J. C.
490 A. Bardwell et al., 1991). Proteins that require disulfide bond formation between nonconsecutive
491 cysteines undergo further processing through the activity of disulfide isomerases (DsbC and
492 DsbG) that rearrange these bonds (Berkmen et al., 2005; Hiniker & Bardwell, 2004; Manta et
493 al., 2019).
494

495 In *P. aeruginosa*, homologs of the regulatory two-component system *dsbRS* have been
496 shown to regulate the activation of *dsbDEG* homologs partly by binding copper ions (Yu et al.,
497 2022). Based on this study, we predict that evolved *dsbS* mutants lead to altered

498 phosphorylation of *dsbR* which interferes with its regulation of *dsbDEG*. The evolved intergenic
499 mutation is found in the predicted DsbR binding site and would therefore reduce *dsbDEG*
500 transcription. The evolved DsbE-DsbG fusion mutant likely interferes with the ability of these
501 proteins to fold properly, with the downstream consequence of misfolded periplasmic proteins.
502 Taken together, we predict that all mutations in this pathway result in misfolded periplasmic
503 proteins, although the exact proteins that are affected are unknown. Interestingly, in *P.*
504 *aeruginosa*, deletion of *dsbA* led to a small colony variant phenotype that was hypothesized to
505 be a result of YfiR misfolding due to its cysteine residues that contribute to dimerization,
506 resulting in constitutive activation of YfiN and elevated cyclic-di-GMP (Malone et al., 2012).
507 However, the small colonies produced by *dsb* mutations differ from the wrinkly mutants of
508 caused by *yfiR* mutations, suggesting different effects on biofilm requiring further study.
509

510 **Discovery of frequent mutations in phosphodiesterase *bmo* that do not change colony**
511 **morphology**

512 Clones retaining the ancestral, smooth colony phenotype at the end of evolution
513 experiments often acquired a mutation in *bmo*, a gene with both DGC and PDE domains that is
514 highly conserved in the genus *Pseudomonas* and predicted to function primarily as a PDE (Fig.
515 3) (Eilers, Hoong Yam, et al., 2024; Wei et al., 2019). A representative mutant showed
516 intermediate levels of both biofilm production and motility, leading us to name this gene *bmo* for
517 its role in balancing both biofilm and motility. We predict that our model selects for *bmo* mutants
518 because they act as biofilm generalists that have improved attachment and biofilm formation
519 compared to their ancestor, while also maintaining the ability to disperse from the old bead to
520 recolonize the new bead. Characterization of multiple biofilm-associated phenotypes supports
521 this hypothesis. Compared to the ancestor and the hyper-biofilm *wspF* mutant, *bmo* has
522 intermediate motility, cyclic di-GMP, and overall biofilm attachment phenotypes, whereas its
523 cellular attachment to the bead is as high as *wspF* (Fig. 5). Moreover, *bmo* biofilm phenotypes
524 are nearly identical to the LPS mutant *fuzY*, although *bmo* has somewhat improved motility,
525 attachment, and overall biofilm formation, along with significantly greater cyclic di-GMP levels. It
526 is also notable that *bmo* mutants appear to be selected more frequently in media containing
527 triclosan, suggesting the stress imposed by this compound interacts with the *bmo* regulatory
528 pathway that remains to be defined.
529

530 *P. aeruginosa bmo* homologs have been shown to influence biofilm formation and
531 regulate basal levels of cyclic di-GMP. A deletion mutant of the *P. aeruginosa* PA14 homolog
532 (PA14_03720) had reduced swimming motility and increased twitching motility in comparison to
533 wild-type PA14 (Ha et al., 2014). Deletion mutants of the *P. aeruginosa* PAO1 homolog
534 (PA0285, *pipA*) have increased biofilm formation, aggregation, Psl production, and cyclic di-
535 GMP production, and decreased swimming motility (Cai et al., 2022; Eilers et al., 2022; Wei et
536 al., 2019). A recent study that compared deletion mutants of *bmo* homologs in *P. aeruginosa*
537 strains PA01, PAK, and PA14, and *P. putida* strain KT2440 found that these mutants had
538 increased early attachment (at 4, 6, and 8 hours) in comparison to their wild-type counterparts
539 and that the magnitude of these differences depended on strain background (Eilers, Hoong
540 Yam, et al., 2024). Among the 22 unique mutants detected by deep sequencing populations
541 evolved in the bead biofilm model, most are predicted to (1) cause loss-of-function by
542 introducing premature stop codons or (2) negatively affect PDE function or PAS domain
543 signaling through nonsynonymous SNPs (Sup. Table 1). We predict these mutants resemble
544 the representative mutant clone we studied (Fig. 5) by having a higher basal level of cyclic di-
545 GMP that improves their attachment to the bead surface and biofilm formation.
546
547 **Phenotypic differentiation among mutants reflects niche differentiation that enables**
548 **coexistence**
549 The spectrum of biofilm phenotypes arising in these experiments suggests that they
550 exploit different ecological conditions, which could explain both their rapid emergence and
551 subsequent coexistence. This model was well supported by confocal microscopy of biofilms
552 produced by individual mutants and mixed pairs (Fig. 6, Fig. S3) but these measurements were
553 on glass rather than polystyrene and did not allow mutants to reach equilibrium frequencies.
554 Therefore, we mixed representative mutants of each morphology and tracked their frequencies
555 over a week of passage. The *bmo* mutant and the ancestor appeared to compete as their
556 intermediate frequencies oscillated, whereas *wspF* and *fuzY* mutants rapidly declined but were
557 maintained at low (~5-10%) frequencies (Fig. 7). The cycling between the *bmo* mutant and the
558 ancestor can be explained by their occupying overlapping but distinct niches (Brisson, 2018;
559 Chesson, 2000), whereas the persistence of *wspF* and *fuzY* at lower frequencies suggests they
560 inhabit more differentiated biofilm niches but are outcompeted by the other genotypes under
561 most conditions (Fig. 6, Fig. S3, Table 2). These dynamics agreed with the phenotypic

562 dynamics from the 15-day evolution experiment (Figure 4), in which biofilm-adapted mutants
563 with distinct wrinkly and fuzzy colony morphologies rapidly arose and persisted at low
564 frequencies while ancestral colony morphologies consistent with persistence of the ancestor
565 and biofilm-adapted *bmo* mutants predominated. These overall interactions conform to a model
566 known as multi-niche selection (Levins, 1963), which requires that each species has a selective
567 advantage in some habitats while others are superior in other habitats, with areas of niche
568 overlap. We suggest that the repeated emergence and maintenance of genotypes with
569 differentiated niches within the biofilm life cycle provides a clear example of how variable
570 environments can favor balanced polymorphisms (Martin et al., 2016; Poltak & Cooper, 2011).
571 Given the ubiquity of microbial biofilms undergoing regular cycles of attachment, aggregation,
572 dispersal, and reattachment, we can expect genetic and phenotypic heterogeneity like that
573 shown here to be widespread. This diversity may therefore be expected in biofilms produced by
574 natural populations of *P. fluorescens* in and around plants or in those produced by its relative *P.*
575 *aeruginosa* in the built environment or when establishing opportunistic infections.
576

577 **Building a community of learners studying biofilm evolution who understand its**
578 **biomedical relevance**

579 We began the EvolvingSTEM project in 2013 with the aim of teaching evolution and
580 genetics in high school classrooms through an authentic bacterial evolution experiment. Our
581 rationale was that the predominant way of teaching natural selection through passive, historical
582 examples of speciation would be less effective than the experience of seeing evolution in action
583 in student-led experiments. We showed that high school students achieved greater learning of
584 content meeting Next Generation Science Standards (States, 2013) in a prior study (Cooper et
585 al., 2019). But this work also held promise for expanding our understanding of mechanisms of
586 biofilm adaptation, given the increasing speed and economy of genotyping mutants by whole-
587 genome sequencing. As we collected these mutants and identified their genetic causes, we
588 added these discoveries into our curriculum materials and emphasized how these mutants
589 reinforced and extended our understanding of how *P. fluorescens* and its pathogenic relative *P.*
590 *aeruginosa* adapt when biofilm formation is advantageous. Mutations in the *wsp* cluster, in
591 *yfiBNR*, and in *morA* are commonly recovered in infections caused by *P. aeruginosa* (Gloag et
592 al., 2019; Malone et al., 2010; Marvig et al., 2015; Smith et al., 2006), and their recovery here
593 indicates their centrality to this lifestyle switch. In addition, our discovery of mutants in *fuzY* adds

594 to evidence that LPS alterations enhance aggregation and potentially alter susceptibility to
595 bacteriophage (Ferguson et al., 2013), and mutants in the *dsb* pathway and *bmo* highlight less
596 understood genetic pathways to biofilm production that warrant more research into how
597 *Pseudomonas* senses surfaces and initiates attachment.
598 The experience of offering this curriculum in subsequent years at more than 30 middle
599 and high schools suggests broader and potentially more potent benefits, including improved
600 student attitudes towards science and technology and greater student confidence as science
601 learners, which we have and will report elsewhere (Quigley et al., 2025). One reason that
602 students may begin to see themselves as scientists is the peer reinforcement from collaborating
603 in small groups to conduct the experiments and as an entire class to discuss their findings.
604 Likewise, often multiple classes per school participate in EvolvingSTEM, and within Pittsburgh
605 Public Schools, twelve different schools conducted these experiments in 2024. This article
606 synthesizes their discoveries and we hope encourages greater sharing of student discoveries
607 among more than 2500 students annually who learn about the medical and natural relevance of
608 microbial biofilms from our curriculum. They complete their experiments knowing that the
609 mutants they identify may contribute to a greater understanding of how bacteria evolve in
610 biofilms and ultimately how to manage these evolving communities.
611
612

613 **MATERIALS & METHODS**

614

615 **School bacterial growth conditions**

616 Students cultured *Pseudomonas fluorescens* strain SBW25, a plant-colonizing bacteria
617 that was isolated in 1989 from the leaf surface of a sugar beet plant grown at the University
618 Farm (Whytham, Oxford, UK) (Bailey & Thompson 1992; Rainey & Bailey 1996 Molecular
619 Microbio). Students cultured bacteria in test tubes that contained 5mL of Queen's B growth
620 media (Cooper et al. 2019, 20g Proteose Peptone No. 3, 1.5g Potassium Phosphate Dibasic,
621 25mL Glycerol, and 6mL 1M Magnesium Sulfate per liter) and a polystyrene bead and plated
622 their bead-attached bacterial populations on Half-Strength Tsoy-Agar plates (15g Tsoy and 15g
623 Agar per liter) at the beginning and end of the experiment. In addition, 25µg/mL of the broad-
624 spectrum antimicrobial triclosan was added to the media and agar plates used in the
625 experiments at SciTech and Allderdice to inhibit bacterial and fungal contamination.
626 *Pseudomonas* species are naturally resistant to triclosan, and this concentration was chosen
627 because it is used in *Pseudomonas* isolation agar (e.g., Cat# 17208 Pseudomonas Isolation
628 Agar from Millipore Sigma).

629

630 WHS students grew *P. fluorescens* cultures for 13 days at 28 °C on a roller drum under
631 biofilm selection conditions, which included 7 bead transfers. SciTech and Allderdice students
632 grew cultures for 4 days on an orbital shaker at 150rpm under biofilm selection conditions,
633 which included 3 bead transfers. SciTech students grew their cultures at 28 °C, while Allderdice
634 students grew their cultures at room temperature because they did not have an available
635 incubator.

636

637 **Genome sequencing and identification of mutants**

638 Clones were selected from the final plating day of the EvolvingSTEM classroom
639 experiment and grown overnight in 5mL QB media. DNA was extracted from 1mL of the
640 overnight culture with the DNeasy Blood and Tissue Kit (Qiagen). Illumina whole-genome
641 sequencing was performed by our laboratory to a minimum depth of 40x coverage on an
642 Illumina NextSeq500 using the methods described in Baym et al. 2015. Trimmomatic (Bolger et
643 al. 2014) was used to remove sequence adaptors, along with low-quality sequence fragments.
644 We identified mutations by comparing evolved clones to the published genome of *P. fluorescens*

645 SBW25 (NCBI Reference Sequence: NC_012660) using breseq (Deatherage and Barrick
646 2014). All sequencing data are available at NCBI Bioproject PRJNA1284392.
647
648 The ancestral *P. fluorescens* SBW25 populations all exhibited a smooth colony
649 morphology phenotype. In comparison to the published genome sequence, the ancestor used
650 by all student populations had three intergenic mutations present in their ancestral populations:
651 (1) +G at position 45,881; (2) +C at position 985,333; and (3) $C_{5\rightarrow3}$ at position 3,447,984. The
652 ancestor used by WHS in 2015 also had a 129bp deletion at position 360,368 and an 132bp
653 deletion at position 6,223,020.
654
655 **Experimental evolution and longitudinal whole-population sequencing**
656 Populations were initiated with a single *P. fluorescens* SBW25 ancestral clone and
657 evolved for 15 days (14 transfers) in 2mL Queen's B growth medium at 28°C on an orbital
658 shaker at 150rpm. Four replicate lineages were propagated under two biofilm conditions: biofilm
659 selection + 25µg/mL triclosan and biofilm selection without triclosan. Biofilm lineages were
660 propagated using four beads each (following the methods of (Santos-Lopez et al., 2019;
661 Scribner et al., 2020). After 24 hours growth, one bead was transferred to a new test tube with
662 three new beads.
663 To perform whole-population sequencing, we collected bead-attached bacteria on days
664 3 and 15 by transferring two beads from each population to a tube with 1.2mL PBS, which was
665 vortexed for 2 minutes to release bacteria from the beads. 500uL was immediately centrifuged
666 for 10 minutes at 14,000rpm, the supernatant was removed, and pellets were stored at -20C for
667 DNA extraction. Sequencing libraries were prepared to a minimum read depth of 150x coverage
668 and analyzed as above with the additional "-p" polymorphism flag in breseq to characterize all
669 reliable mutations at intermediate frequencies in these populations.
670
671 **Motility Assays**
672 Assays were performed as described in Filloux and Ramos (2014). Images were
673 analyzed with FIJI (Schindelin et al., 2012). For swarming motility, we grew 6-hour cultures in
674 LB-Lennox Broth (10g Tryptone, 5g Yeast Extract, 5g NaCl per L) at 28°C, 150rpm, then
675 inoculated Swarming Motility Agar Plates (0.6% agar, 1x M8 solution, 0.2% glucose, 0.5%
676 casamino acids, 1mM $MgSO_4$) with 2.5µL culture pipetted onto the center of the plate, at the

677 surface of the agar. Plates were incubated upright at room temperature (~22°C) for 16-24 hours
678 and photographed. For swimming motility, we grew 6-hour cultures of *P. fluorescens* in LB-
679 Lennox Broth at 28C, 150rpm, transferred 100μL to a 1.5mL microcentrifuge tube, dipped a
680 200uL pipette tip into the culture and used this to stab into the center of Swimming Motility Agar
681 Plates (same recipe as Swarming Motility Plates, but with 0.3% agar). Plates were incubated
682 upright at room temperature (~22°C) for 16-24 hours and photographed. For twitching motility,
683 we stabbed a match-head sized inoculum from a 2-day old streak plate into the center of an LB-
684 Lennox Agar Plate (10g Tryptone, 5g Yeast Extract, 5g NaCl, 10g Agar, 0.5g Tetrazolium Red,
685 per L) all the way down to the plastic. Plates were inverted and stored in stacks of 3 or less in a
686 plastic box lined with wet paper towels at 28°C with box lid slightly ajar for 24 hours and
687 photographed.
688
689 **Biofilm assays**
690 Our biofilm assay is based on the bead model developed by our lab for studying biofilm
691 formation and evolution. Bacterial cultures were inoculated in triplicate in 2 mL of Queen's B
692 media and two plastic beads (Cospheric, Polystyrene Spheres, 7.00mm +/- 0.025mm) and
693 grown overnight at 150 rpm on an orbital shaker at 28°C. Each culture was sonicated for 10
694 seconds at 30% amplitude and used to inoculate two new cultures at a 1:100 dilution in QB both
695 with and without 30 μg/mL triclosan and two polystyrene beads. Cultures were then grown for
696 24 hours on an orbital shaker at 28°C, 150 rpm, serial diluted, and plated. Biofilm formation was
697 quantified by transferring one of the two beads to a single well of a 24-well plate with 1.5mL of
698 an 0.1% crystal violet solution and incubated at room temperature for 15 minutes. The bead was
699 then washed three times in water for one minute each time to remove excess crystal violet.
700 Biofilm-bound crystal violet was then solubilized by vortexing the bead for 2 minutes in a 2mL
701 tube filled with 1mL solubilization solution: 95% ethanol, 4.95% water, 0.05% Triton X-100. The
702 concentration of crystal violet was measured at an absorbance wavelength of 590 nm (OD590).
703 Total colony forming units per bead were determined by serial diluting and plating bacteria
704 attached to the second bead. We adopted this method to (1) more accurately represent the
705 conditions in which we grow biofilms in our experiments and (2) allow us to differentiate
706 between total biofilm production and bacterial attachment to the bead. As an indicator of EPS
707 production, we plated mutants on half-strength T-Soy Agar plates (15g Tsoy, 15g Agar, 0.02g

708 Congo Red, 0.0075g Brilliant Blue per liter) and visually assessed dye uptake, where dark red
709 colonies indicate EPS overproduction.
710
711 **Intracellular cyclic di-GMP Assay**
712 The *P. fluorescens* ancestor and biofilm-adapted mutants were transformed with the
713 cyclic di-GMP reporter plasmid, pCdrA-gfpC (Addgene plasmid #111614) (Rybtke et al., 2012).
714 The reporter transcriptionally fuses the *P. aeruginosa* PA01 *cdrA* promoter, which is responsive
715 to cyclic di-GMP, to genes encoding green fluorescent protein. Starter cultures of each
716 transformed *P. fluorescens* genotype and an untransformed ancestor control were grown in their
717 own cultures of 2 mL of Queen's B media at 28°C on an orbital shaker at 150 rpm for 24 hours.
718 Following this, experimental cultures containing 4 mL of Queen's B media were inoculated with
719 10 μL of a given starter culture and incubated at 28°C on an orbital shaker at 180 rpm for 24
720 hours. After incubation, a 100 μL sample of each experimental culture was used to capture
721 fluorescence intensity and OD_{600}. Cyclic di-GMP levels at 24 hours were calculated by
722 $\ln(RFI)/\ln(ROD_{600})$, where RFI is relative fluorescence intensity (the ratio of absolute
723 fluorescence intensity of experimental to control culture), and ROD_{600} is relative optical density
724 (the ratio of absolute optical density at a wavelength of 600 nm of a bacterial culture to fresh
725 media).
726
727 **Construction of fluorescently tagged *P. fluorescens* strains**
728 A single colony of *P. fluorescens* was inoculated into 5 ml QB and grown overnight to stationary
729 phase. One mL of culture was pelleted by centrifugation and washed twice with 300 mM
730 sucrose. After resuspending the pellet in 100 uL of 300 mM sucrose, 5 uL pTNS3 and 5 uL of
731 the desired pBT plasmid (Table S3) were added and the suspension was incubated at room
732 temperature for 5 minutes. The suspension was then transferred to an electroporation cuvette (2
733 mm gap) and pulsed at 2.5 kV. Cells were recovered in 1 mL LB and transformants were
734 selected on LB agar + 30 ug/mL gentamicin at 28˚C.
735
736 **Confocal microscopy**
737 *P. fluorescens* strains expressing eGFP or mCherry were pre-cultured for 24 hours in
738 glass-bottom plates containing 2 mL of Queen's B media and shaken on an orbital shaker at a
739 speed of 125 rpm. Biofilms generated by *P. fluorescens* were expected to attach to the surface

740 of the glass. After pre-culture, the old media in the plates were removed by pipetting, and the
741 biofilms were washed twice with 1 mL of PBS to remove excess planktonic bacterial cells.
742 Following the washing step, 1 mL of fresh PBS was added to each glass-bottom plate to
743 maintain the survival and limit the growth of bacterial cells within the biofilm. Images were
744 captured at 400× magnification in both eGFP and mCherry channels on an Olympus FV-1000
745 confocal microscope. Z-stack images spanned from the bottom to the top of the biofilms. Image
746 processing was conducted using ImageJ (Schindelin et al., 2012) and BiofilmQ (Hartmann et al.,
747 2021).
748
749 **Multi-genotype competition assay**
750 We created mixed populations of bacteria by combining a representative mutant of *bmo*
751 (PFLU0185) (with a single nucleotide insertion resulting in a premature stop codon truncating
752 both the DGC and PDE domains), wrinkly (*wspF* Q185*) and fuzzy (*fuzY* Q11*) mutants, along
753 with a lac-marked *P. fluorescens* SBW25 ancestor. All four clones were used to inoculate
754 cultures containing 2mL QB and 2 beads and grown overnight at 28°C on an orbital shaker at
755 150rpm. Both beads were then transferred to 1.5mL QB in small glass tubes and vortexed for 2
756 minutes and this mixture was used to make freezer stocks. Bacteria from a portion of one
757 freezer stock was diluted in QB and 50uL of this dilution was transferred to 6 replicate
758 populations containing 2mL QB and 4 beads. Starting frequencies of each mutant and ancestor
759 were determined by diluting a spread-plating from each starting culture. Populations were then
760 evolved for 4 days (3 transfers) in 2mL Queen's B growth medium at 28°C on an orbital shaker
761 at 150rpm. Every 24 hours, one bead was transferred to a new test tube with three new beads
762 and all newly colonized beads were vortexed for 2 minutes, diluted, and spread-plated to count
763 changes in colony phenotypes over time.
764
765 **ACKNOWLEDGEMENTS**
766 We thank Tyler McAloon and Erin Nawrocki for technical support. We appreciate the
767 commitment of dozens of teachers and thousands of students to implement this curriculum,
768 isolate these mutants, and inspire this research. This work was supported by SEPA
769 R25AI180989 from the NIH, by BIORETS DBI-2147075 from the NSF, and by the Dean's office
770 from the University of Pittsburgh, School of Medicine.
771

772 **Table 1.** Genotypes of *P. fluorescens* mutants determined by WGS that were isolated based on
773 colony phenotype by students in different schools (ST, WHS, A, or Lab = our research lab).
774 *denotes presence of secondary mutations, see Table S2 for details. #denotes representative
775 mutant used in phenotypic studies
776

School (count)	Phenotype	Position (nt)	Mutation	Annotation	Gene
ST#	smooth	210,961	+T	coding (565/1989 nt)	*PFLU0185 (bmo)*
ST	smooth	211,021	C→T	Q209* (CAG→TAG)	*PFLU0185 (bmo)*
ST*	smooth	211,277	+A	coding (881/1989 nt)	*PFLU0185 (bmo)*
ST	smooth	212,132	Δ210 bp	coding (1736-1945/1989 nt)	*PFLU0185 (bmo)*
ST / WHS*	wrinkly	1,353,115	Δ84 bp	coding (846-929/1623 nt)	*PFLU1219 (wspA)*
WHS	wrinkly	1,353,408	T→C	V380A(GTG→GCG)	*PFLU1219 (wspA)*
ST / WHS (2)	wrinkly	1,353,411	C→T	A381V (GCC→GTC)	*PFLU1219 (wspA)*
ST	wrinkly	1,355,373	Δ335 bp	fusion of 2 predicted ORFs	*[PFLU1221(wspC)] –[PFLU1222(wspD)]*
WHS	wrinkly	1,358,709	G→C	A32P (GCC→CCC)	*PFLU1224 (wspF)*
WHS (3)*	wrinkly	1,358,766	Δ15bp	coding(151-165/1011nt)	*PFLU1224 (wspF)*
WHS (3)	wrinkly	1,358,780	$(CTGATGG\ ACCTGATC)_{1\rightarrow2}$	coding (165/1011 nt)	*PFLU1224 (wspF)*
WHS	wrinkly	1,358,846	Δ18bp	coding(231-248/1011nt)	*PFLU1224 (wspF)*
WHS	wrinkly	1,358,893	Δ27 bp	coding (278-304/1011 nt)	*PFLU1224 (wspF)*
WHS (3)	wrinkly	1,358,989	+A	coding (374/1011 nt)	*PFLU1224 (wspF)*
WHS	wrinkly	1,359,085	G→T	G157V (GGC→GTC)	*PFLU1224 (wspF)*
ST# / WHS (2)*	wrinkly	1,359,168	C→T	Q185* (CAG→TAG)	*PFLU1224 (wspF)*
WHS	wrinkly	1,359,234	+G	coding (619/1011 nt)	*PFLU1224 (wspF)*
WHS	wrinkly	1,359,292	Δ150bp	coding (677-826/1011nt)	*PFLU1224 (wspF)*
WHS	wrinkly	1,359,330	G→C	A239P (GCC→CCC)	*PFLU1224 (wspF)*
WHS (6)	wrinkly	1,359,364	G→C	R250P (CGG→CCG)	*PFLU1224 (wspF)*
WHS*	wrinkly	1,359,370	C→T	S252L (TCG→TTG)	*PFLU1224 (wspF)*
ST	wrinkly	1,359,446	Δ1 bp	coding (831/1011 nt)	*PFLU1224 (wspF)*
WHS (2)	wrinkly	1,359,495	A→C	T294P (ACC→CCC)	*PFLU1224 (wspF)*
WHS (3)	wrinkly	1,359,538	C→T	P308L(CCC→CTC)	*PFLU1224 (wspF)*
WHS	wrinkly	1,359,552	$(GCG)_{4\rightarrow3}$	coding (937-939/1011 nt)	*PFLU1224 (wspF)*
WHS	wrinkly	1,359,554	$(GCG)_{4\rightarrow5}$	coding (939/1011 nt)	*PFLU1224 (wspF)*

ST (3)	small	4,830,895	$(GCAGGC)_{2\rightarrow1}$	coding (8-13/1323 nt)	*PFLU4380 (dsbS)*
ST	small	4,834,252	Δ110 bp	fusion of 2 predicted ORFS	*[PFLU4383]–[PFLU4384 (dsbG)]*
ST	wrinkly	5,707,197	G→A	Q157* (CAA→TAA)	*PFLU5211 (awsX/YfiR)*
ST	wrinkly	5,707,256	A→C	I137S (ATC→AGC)	*PFLU5211 (awsX/YfiR)*
WHS*	wrinkly	5,707,317	Δ33bp	coding (317-349/573nt)	*PFLU5211 (awsX/YfiR)*
WHS	wrinkly	5,707,334	G→T	A111E (GCG→GAG)	*PFLU5211 (awsX/YfiR)*
ST/WHS (5)*	wrinkly	5,707,411	Δ33 bp	coding (223-255/573 nt)	*PFLU5211 (awsX/YfiR)*
ST (2)	wrinkly	5,857,638	G→A	M992I (ATG→ATA)	*PFLU5329 (mwsR/morA)*
ST (3)	wrinkly	5,857,733	Δ9 bp	coding (3071-3079/3852 nt)	*PFLU5329 (mwsR/morA)*
A (3)*	wrinkly	5,858,369	C→T	A1236V (GCC→GTC)	*PFLU5329 (mwsR/morA)*
Lab#	fuzzy	541,214	C→T	Q11* (CAG→TAG)	*PFLU0478 (fuzY)*
Lab	fuzzy	541,772	Δ13 bp	coding (589-601/1149 nt)	*PFLU0478 (fuzY)*

777

Table 2. Linear regressions of frequencies of *bmo* (PFLU0185) between the ancestor (Afreq), *wsp* mutant (Wfreq), and *fzy* mutant (Ffreq), as shown in Figure S4. The significant negative slopes indicate competition.

Model Equation	Std. Error	t value	R-squared	p-value
Pfreq = (-0.99)Afreq + 0.91	0.07	-14.69	0.79	<0.0001
Pfreq = (-0.7)Wfreq + 0.46	0.32	-2.22	0.08	<0.05
Pfreq = (-1.84)Ffreq + 0.48	0.58	-3.14	0.15	<0.001

Table S1. Complete details of mutant genotypes, including secondary mutations (XLS).

Table S2. Details of mutations detected during the evolution experiment using population-wide whole-genome sequencing (XLS)

Table S3. Plasmids used in this study

Name	Plasmid	Source/Reference
pTNS3	Helper plasmid for site-specific Tn7 transposition	Choi et al. (Choi et al., 2008)
pBT270	pUC18-mini-Tn7T2-PA1/04/03-Gm-GFP	Zhao et al. (Zhao et al., 2013)
pBT277	pUC18-mini-Tn7T2-PA1/04/03-Gm-mCherry	Zhao et al. (Zhao et al., 2013)

794 **FIGURE LEGENDS**

795 **Fig. 1. Biofilm growth patterns and colony morphologies of *P. fluorescens* SBW25**
796 **and evolved biofilm-adapted mutants.** Evolved populations often have a distinct ring of
797 biofilm at the air-liquid interface (A). The *P. fluorescens* ancestor (lac+) has blue, smooth-edged
798 circular colonies (pink circle), the *bmo* (PFLU0185) mutant has yellow, smooth-edged circular
799 colonies (orange circle), the *fuzY* mutant has large, yellow, irregular colonies (yellow circle), and
800 the *wspF* mutant has small, white, irregular colonies (purple circle) (B). Small colony variants
801 (green circle) can be distinguished from their ancestor (pink circle) by their significantly smaller
802 size (B).
803

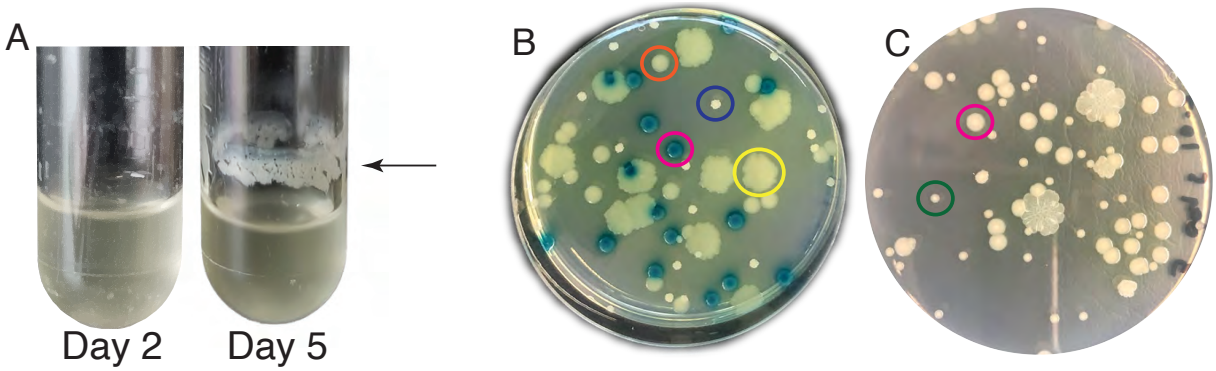

804
805
806

807 **Fig. 2. Wrinkly colony phenotypes are caused by mutations in the *wsp*, *yfiBNR*,**
808 **and *morA* pathways.** Mutations are shown as black bars below the gene diagrams. When
809 multiple independent mutations occurred, their counts are in parentheses. Mutations in *wspF*
810 (31 in total) are too numerous to display. DGC domains are indicated with diagonal hatching;
811 PDE domains are indicated with cross hatching. Genome positions of the beginning and end of
812 each operon/gene are indicated above the gene diagrams. Table 1 and Table S1 contain a
813 complete list of mutations. All mutations are predicted to cause constitutive activation of a DGC,
814 increasing cyclic di-GMP synthesis.

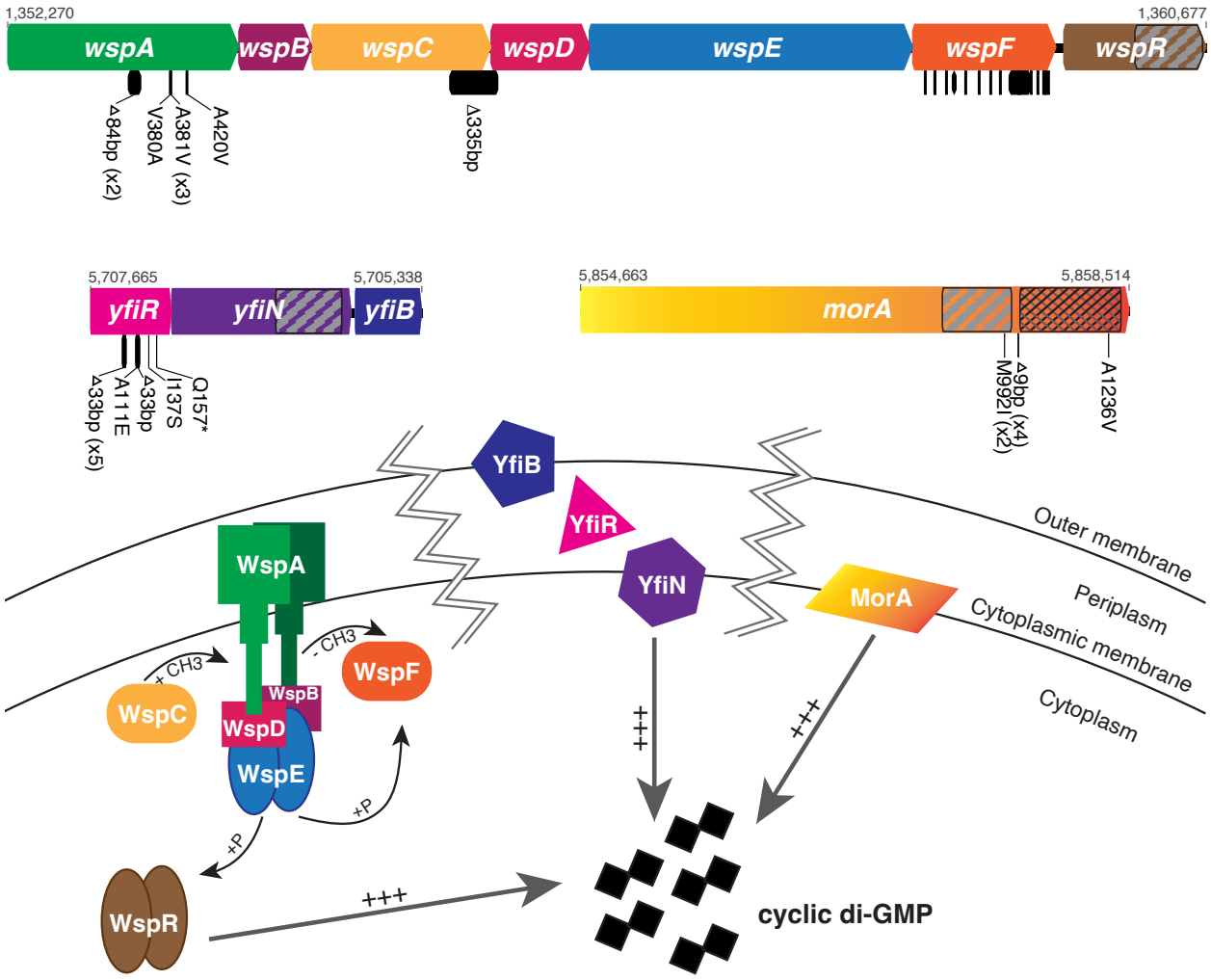

815
816

817 **Fig. 3. Biofilm adaptations caused by mutations in LPS, disulfide bond formation,**
818 **and a novel regulator of cyclic-di-GMP.** Mutations are shown as black bars below the gene
819 diagrams. When multiple independent mutations occurred, their counts are in parentheses.
820 DGC domains are indicated with diagonal hatching; PDE domains are indicated with cross
821 hatching. Genome positions of the beginning and end of each operon/gene are indicated above
822 the gene diagrams. Mutations in *bmo* (PFLU0185) are predicted to increase basal levels of
823 cyclic di-GMP (A). Mutations in *fuzY* are predicted to modify LPS O-antigens (B). Mutations in
824 *dsb* genes are predicted to cause misfolded periplasmic proteins. Table 1 and Table S1 provide
825 mutation details.

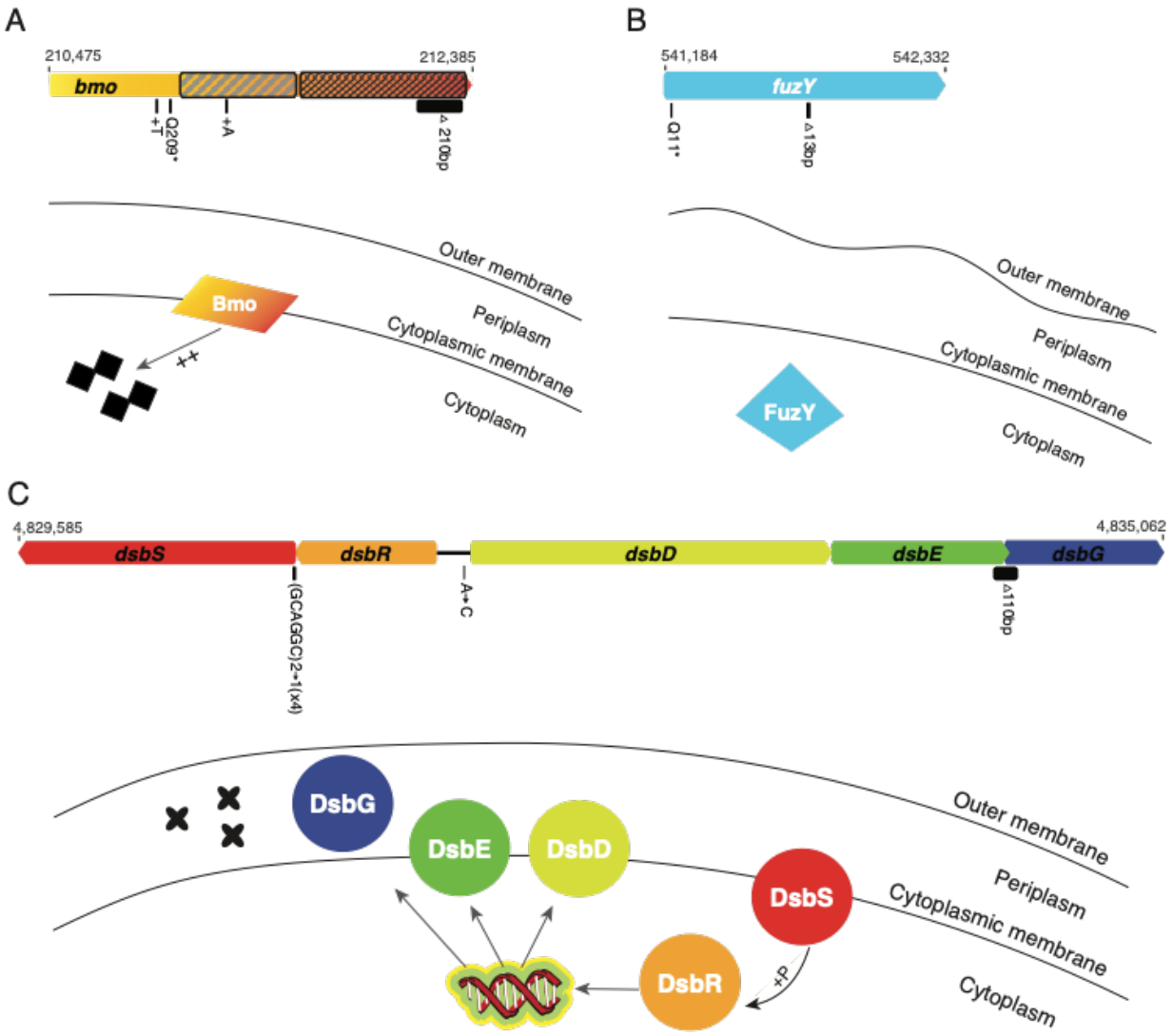

826
827

828 **Fig. 4. Dynamics of evolved phenotypes and genotypes during 15 days of**
829 **experimental biofilm selection.** Populations were grown for 15 days in QB media with or
830 without triclosan with four plastic beads and passaged every 24 hours by transferring one bead
831 into fresh media with three new beads. Bead-attached populations were plated on days 4, 8, 11,
832 and 15 and contained colonies with fuzzy, small, smooth, and wrinkly phenotypes (A). Whole-
833 genome, whole-population sequencing was performed on days 3 and 15. Points include the
834 cumulative frequency of mutations identified in each gene (B). A complete list of mutations can
835 be found in Supplemental Table 1.

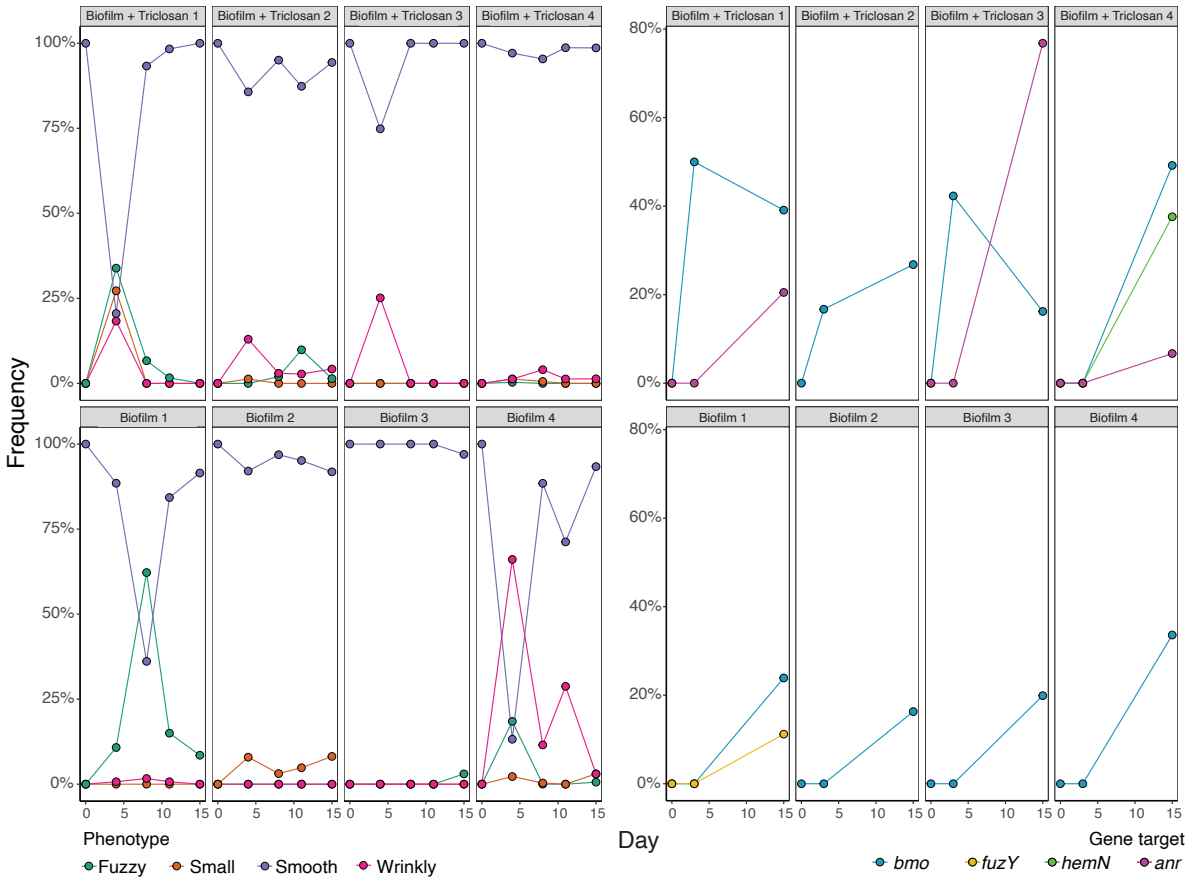

836

837 **Fig. 5. Biofilm-related phenotypes of *P. fluorescens* mutants**. Swarming motility (A)
838 and swimming motility (B) show reduced levels compared to the ancestor. Biofilm production
839 measured by attached colony forming units (C) and by crystal violet absorbance at 590nm (D).
840 Points are the average of three measurements recorded for each replicate. Results in QB media
841 are similar but more pronounced with the addition of triclosan. Relative cyclic di-GMP production
842 from a fluorescent reporter (E) is reported as ln(RFI)/ln(ROD600), where RFI is relative
843 fluorescence intensity and ROD600 is relative optical density. In all panels, mean values are
844 indicated by diamonds, and outliers are indicated by an open circle. Statistical comparisons
845 were conducted by one-way ANOVA with a Games-Howell post hoc test with p = 0.05, with
846 letters at the top of each panel indicating statistically distinct groupings.

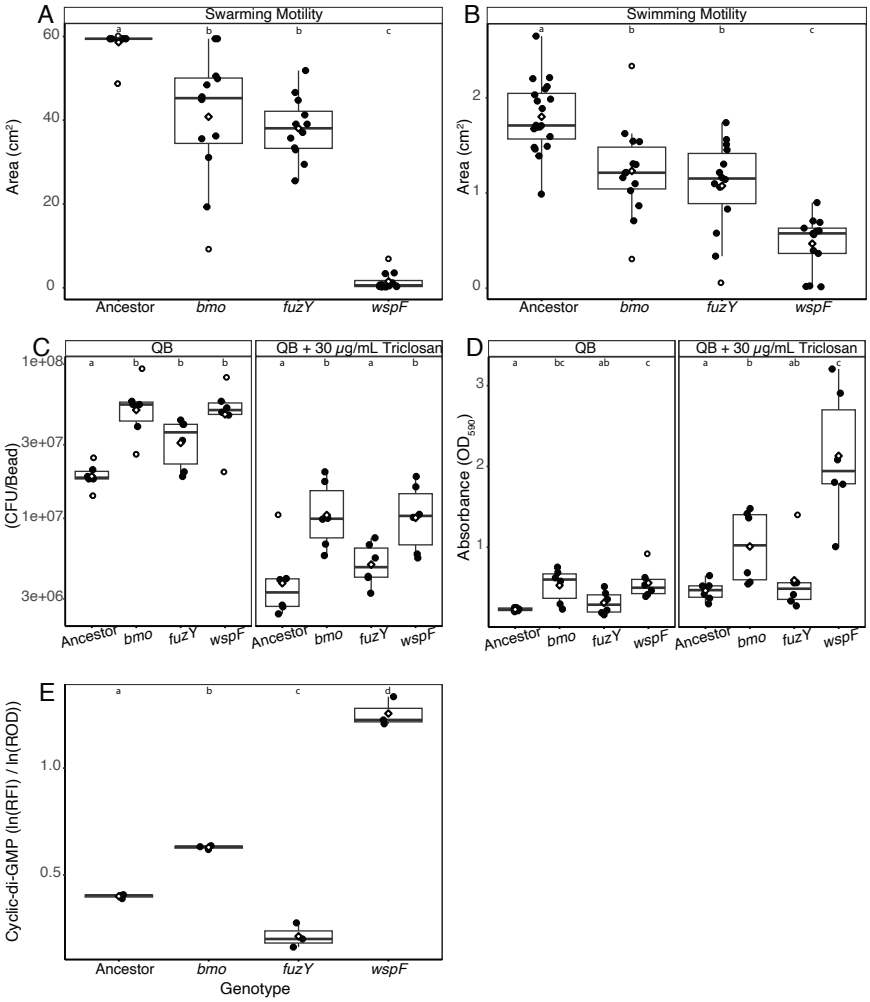

847
848

849 **Fig. 6. Confocal microscopy of representative *P. fluorescens* mutants shows**
850 **differentiated biofilm phenotypes.**. Ancestor (a), *fuzY* (c) and *wspF* (d) are tagged with eGFP
851 and *bmo* (b) is tagged with mCherry. Both Ancestor and *bmo* exhibit uniform biofilm structure.
852 The *fuzY* biofilm is composed of many aggregates. The *wspF* biofilm was in small clusters and
853 was not spatially contiguous on the glass surface, but generated large aggregates in liquid
854 media that were more likely to attach on plastic surfaces (not shown). Mixtures of these mutants
855 were also imaged and are reported in Fig S3.

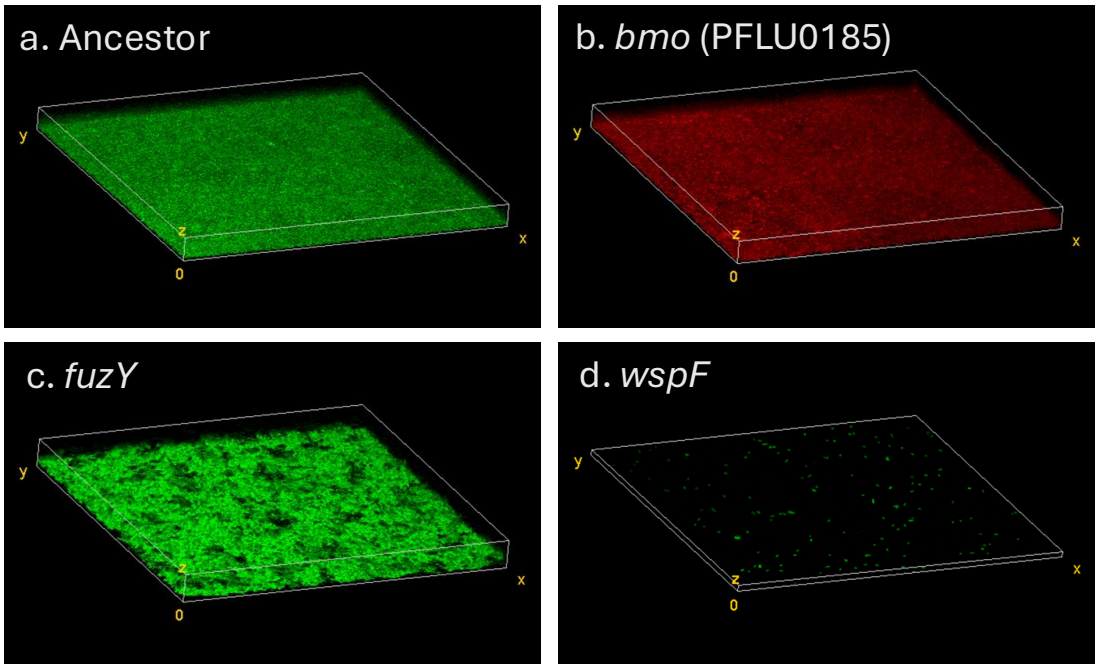

856
857

858 **Fig. 7. Ecological dynamics of constructed communities indicate multi-niche**
859 **selection.** Six populations containing equal volumes of representative, biofilm-adapted loss-of-
860 function mutants in *bmo* (PFLU0185), *fuzY*, and *wspF* were propagated in the biofilm bead
861 model and plated daily to assess frequencies. All mutants persisted, with *fuzY* and *wspF*
862 declining rapidly in frequency and *bmo* and the ancestor fluctuating at intermediate frequencies
863 and opposite trajectories.

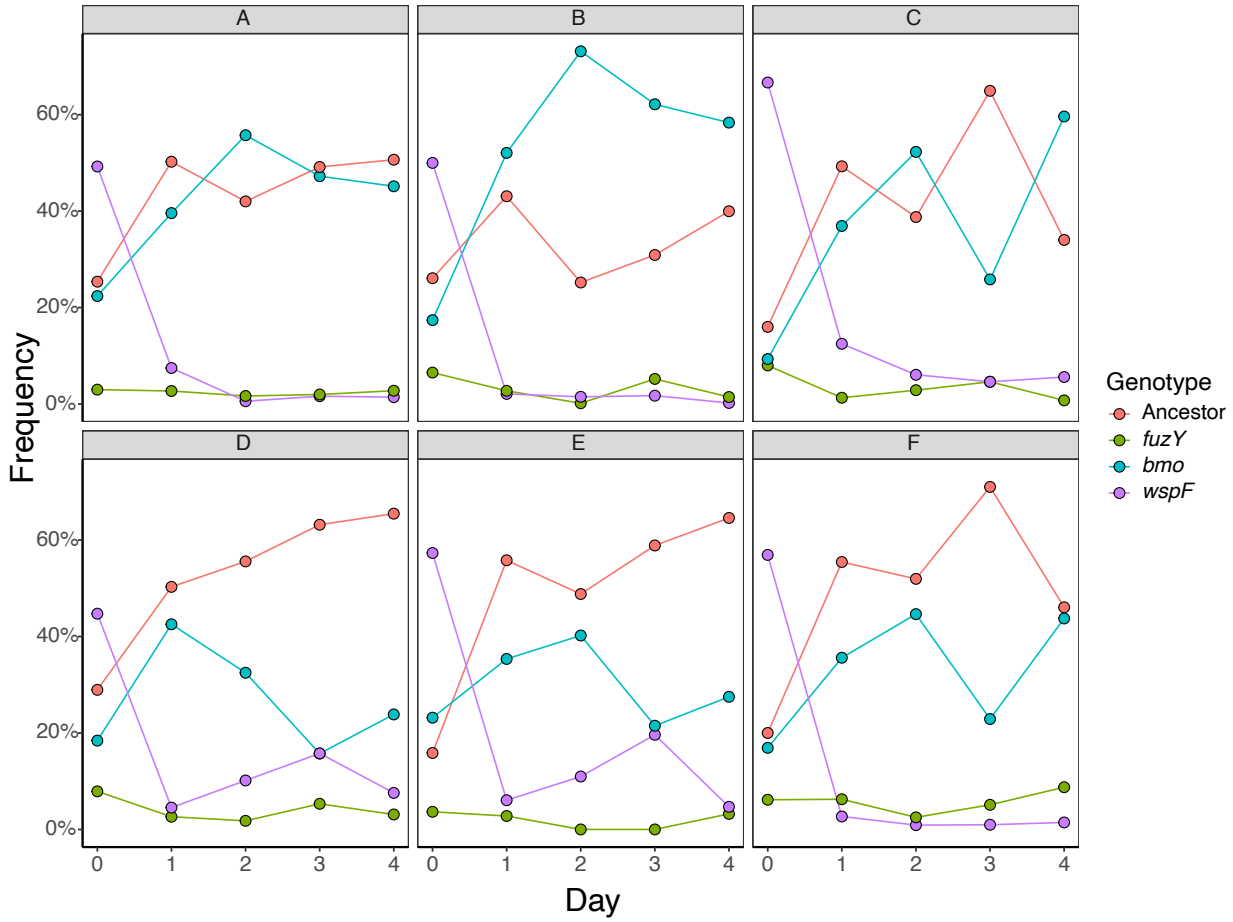

864
865

866 **Fig. S1. *Pseudomonas fluorescens* lacks twitching motility**. Twitching motility was
867 measured on LB-Lennox Agar Plates after 24 hours of growth. PA01 (A) exhibits a twitching
868 phenotype, indicated by the halo surrounding the dark red colony in the center of the plate
869 where inoculation occurred. *P. fluorescens* ancestor (B), *pflu0185* mutants (C), *fuzY* mutants
870 (D), and *wspF* mutants (E) show no signs of twitching motility as all four genotypes lack a halo
871 surrounding the inoculation point.

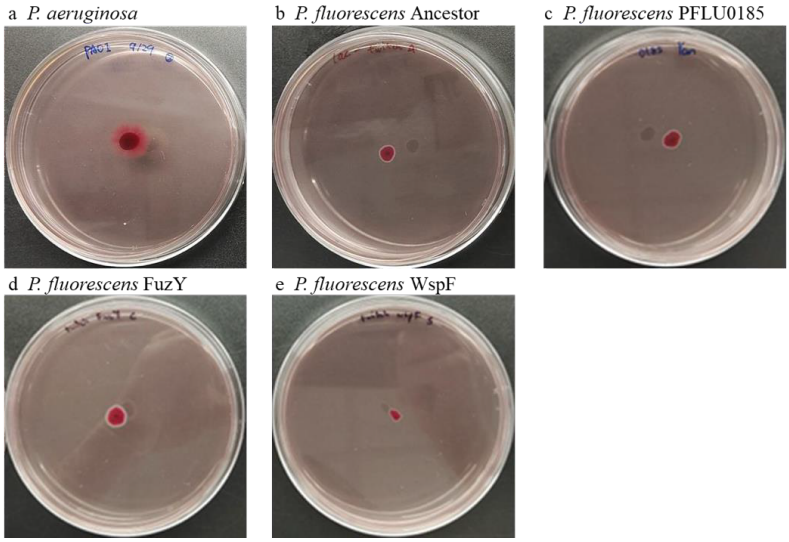

872
873
874

875 **Fig. S2. Planktonic growth is inhibited by triclosan.**

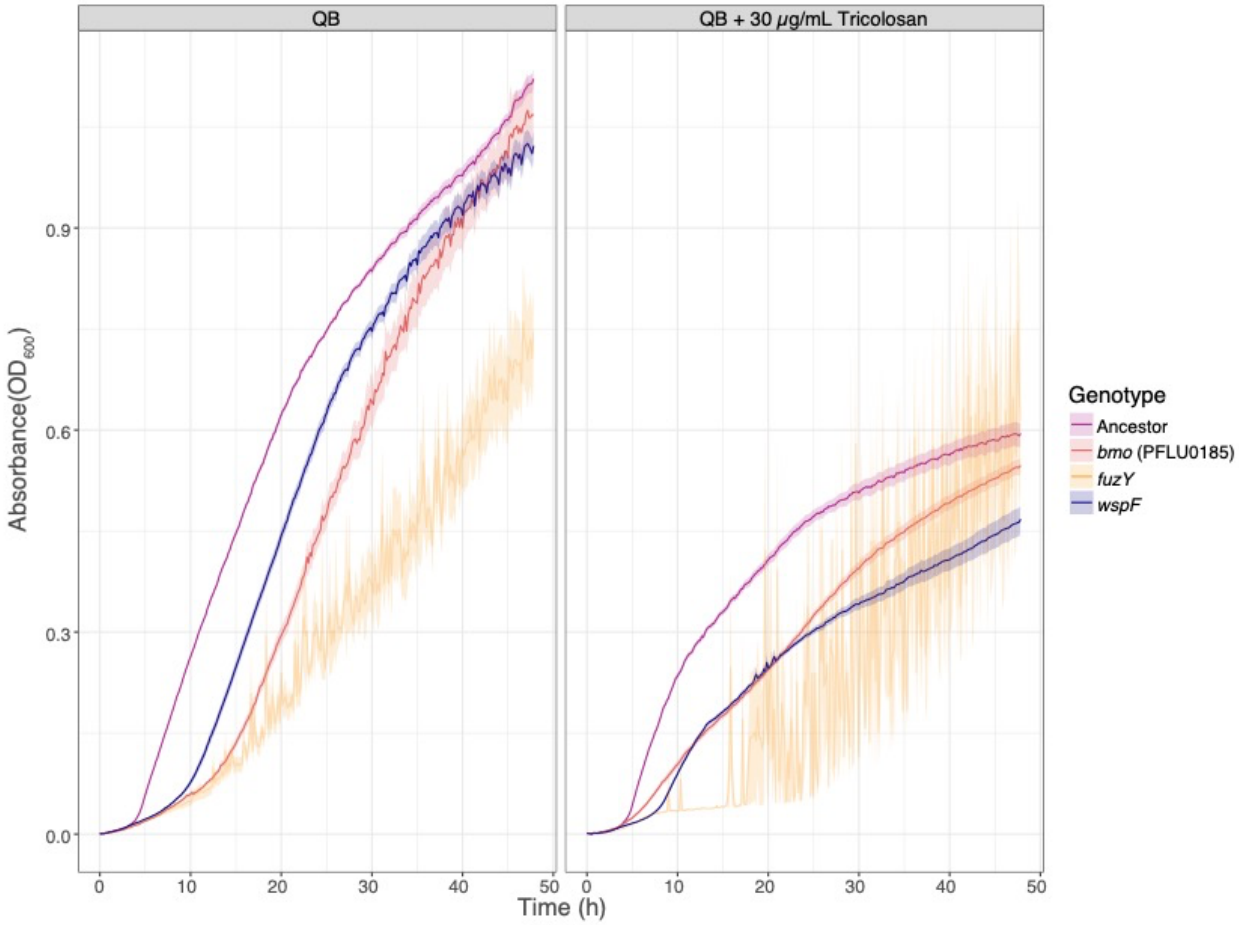

876

877

878 **Fig. S3. Confocal microscopy of representative *P. fluorescens* mutants mixed in**
879 **pairs shows differentiated biofilm phenotypes**. Methods replicate those of Fig 6. Text color
880 of labels indicates fluorescent marker in that genotype; red = mCherry, green = eGFP.

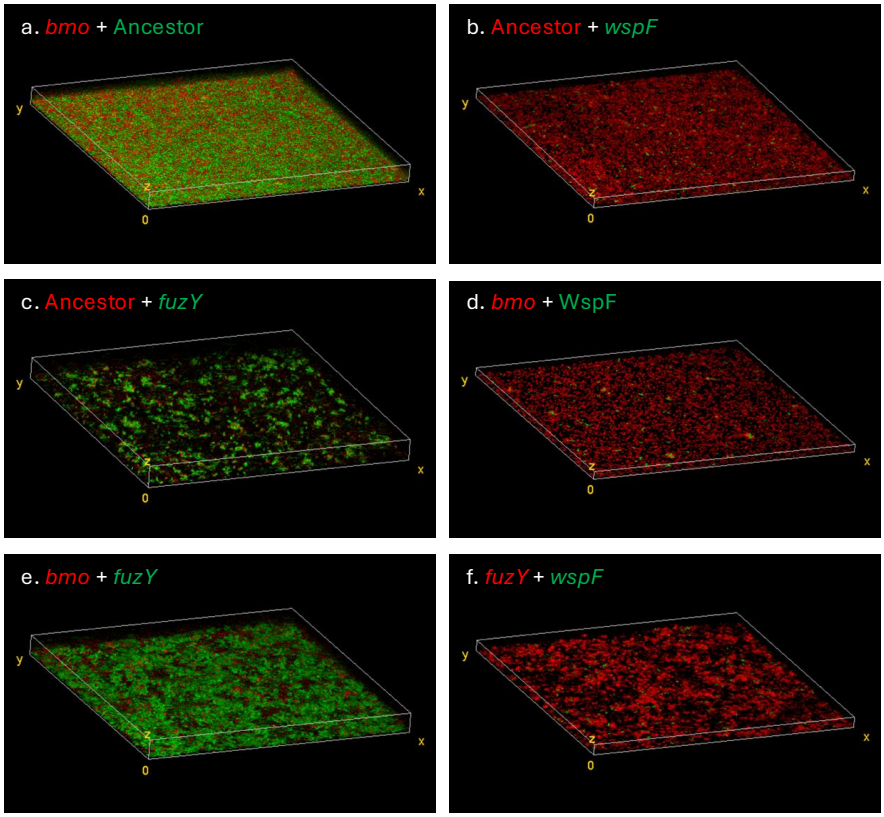

881
882

883 **Fig. S4. Linear regressions of *bmo* frequencies, as compared to ancestor (A),**
884 ***wspF* (B), and *fuzY* (C).**

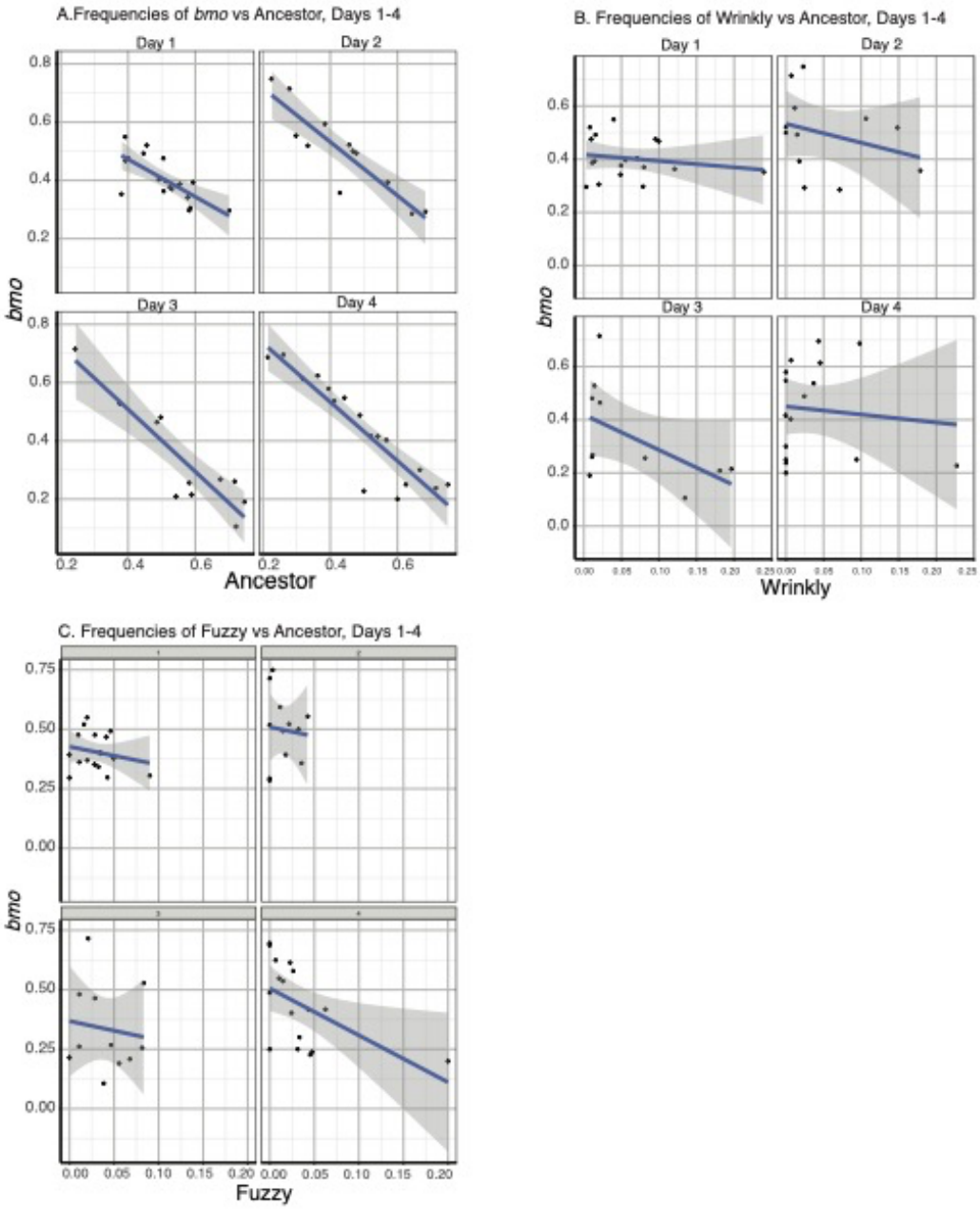

885
886

887 **Fig. S5. Colony morphology of small colony variants with mutations in *dsb* genes**

888 **and their differential uptake of Congo Red dye.**

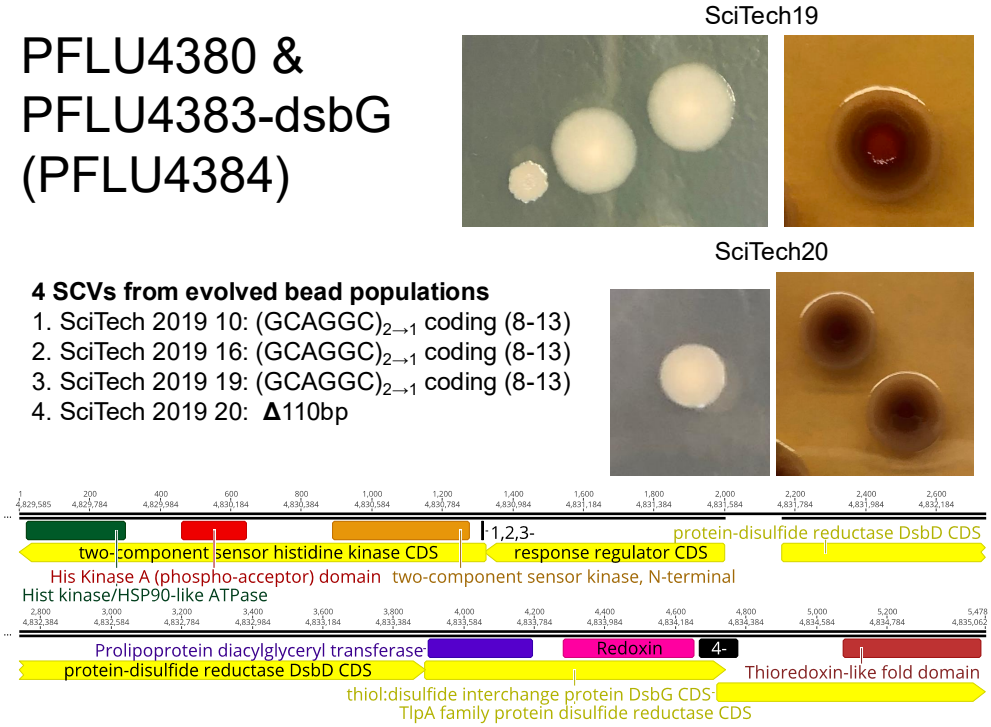

889

890

891

892 **REFERENCES**

893

894 Bader, M. W., Xie, T., Yu, C.-A., & Bardwell, J. C. A. (2000). Disulfide Bonds Are Generated by
895 Quinone Reduction *. *Journal of Biological Chemistry*, *275*(34), 26082–26088.
896 https://doi.org/10.1074/jbc.M003850200

897 Bantinaki, E., Kassen, R., Knight, C. G., Robinson, Z., Spiers, A. J., & Rainey, P. B. (2007).
898 Adaptive Divergence in Experimental Populations of Pseudomonas fluorescens. III.
899 Mutational Origins of Wrinkly Spreader Diversity. *Genetics*, *176*(1), 441–453.
900 https://doi.org/10.1534/genetics.106.069906

901 Bardwell, J. C. A., McGovern, K., & Beckwith, J. (1991). Identification of a protein required for
902 disulfide bond formation in vivo. *Cell*, *67*(3), 581–589. https://doi.org/10.1016/0092-
903 8674(91)90532-4

904 Bardwell, J. C., Lee, J. O., Jander, G., Martin, N., Belin, D., & Beckwith, J. (1993). A pathway for
905 disulfide bond formation in vivo. *Proceedings of the National Academy of Sciences*,
906 *90*(3), 1038–1042. https://doi.org/10.1073/pnas.90.3.1038

907 Berkmen, M., Boyd, D., & Beckwith, J. (2005). The Nonconsecutive Disulfide Bond of
908 Escherichia coli Phytase (AppA) Renders It Dependent on the Protein-disulfide
909 Isomerase, DsbC *. *Journal of Biological Chemistry*, *280*(12), 11387–11394.
910 https://doi.org/10.1074/jbc.M411774200

911 Brisson, D. (2018). Negative Frequency-Dependent Selection Is Frequently Confounding.
912 *Frontiers in Ecology and Evolution*, *6*. https://doi.org/10.3389/fevo.2018.00010

913 Cai, Y.-M., Yu, K.-W., Liu, J.-H., Cai, Z., Zhou, Z.-H., Liu, Y., Wang, T.-F., & Yang, L. (2022).
914 The c-di-GMP Phosphodiesterase PipA (PA0285) Regulates Autoaggregation and Pf4
915 Bacteriophage Production in Pseudomonas aeruginosa PAO1. *Applied and*
916 *Environmental Microbiology*, *88*(12), e00039-22. https://doi.org/10.1128/aem.00039-22

Caplat, P., Anand, M., & Bauch, C. (2008). Symmetric competition causes population oscillations in an individual-based model of forest dynamics. *Ecological Modelling*, *211*(3), 491–500. https://doi.org/10.1016/j.ecolmodel.2007.10.002

Chesson, P. (2000). Mechanisms of Maintenance of Species Diversity. *Annual Review of Ecology, Evolution, and Systematics*, *31*(Volume 31, 2000), 343–366. https://doi.org/10.1146/annurev.ecolsys.31.1.343

Choi, K.-H., Mima, T., Casart, Y., Rholl, D., Kumar, A., Beacham, I. R., & Schweizer, H. P. (2008). Genetic Tools for Select-Agent-Compliant Manipulation of Burkholderia pseudomallei. *Applied and Environmental Microbiology*, *74*(4), 1064–1075. https://doi.org/10.1128/AEM.02430-07

Cooper, V. S., Staples, R. K., Traverse, C. C., & Ellis, C. N. (2014). Parallel evolution of small colony variants in Burkholderia cenocepacia biofilms. *Genomics*, *104*(6, Part A), 447–452. https://doi.org/10.1016/j.ygeno.2014.09.007

Cooper, V. S., Warren, T. M., Matela, A. M., Handwork, M., & Scarponi, S. (2019). EvolvingSTEM: A microbial evolution-in-action curriculum that enhances learning of evolutionary biology and biotechnology. *Evolution: Education and Outreach*, *12*(1), 12. https://doi.org/10.1186/s12052-019-0103-4

Eilers, K., Hoong Yam, J. K., Liu, X., Goh, Y. F., To, K.-N., Paracuellos, P., Morton, R., Brizuela, J., Hui Yong, A. M., Givskov, M., Freibert, S.-A., Bange, G., Rice, S. A., Steinchen, W., & Filloux, A. (2024). The dual GGDEF/EAL domain enzyme PA0285 is a *Pseudomonas* species housekeeping phosphodiesterase regulating early attachment and biofilm architecture. *Journal of Biological Chemistry*, *300*(2), 105659. https://doi.org/10.1016/j.jbc.2024.105659

Eilers, K., Kuok Hoong Yam, J., Morton, R., Mei Hui Yong, A., Brizuela, J., Hadjicharalambous, C., Liu, X., Givskov, M., Rice, S. A., & Filloux, A. (2022). Phenotypic and integrated analysis of a comprehensive Pseudomonas aeruginosa PAO1 library of mutants lacking cyclic-di-GMP-related genes. *Frontiers in Microbiology*, *13*. https://doi.org/10.3389/fmicb.2022.949597

Eilers, K., Yam, J. K. H., Liu, X., Goh, Y. F., To, K.-N., Paracuellos, P., Morton, R., Brizuela, J., Yong, A. M. H., Givskov, M., Freibert, S.-A., Bange, G., Rice, S. A., Steinchen, W., & Filloux, A. (2024). The dual GGDEF/EAL domain enzyme PA0285 is a Pseudomonas species housekeeping phosphodiesterase regulating early attachment and biofilm architecture. *Journal of Biological Chemistry*, *300*(2). https://doi.org/10.1016/j.jbc.2024.105659

Ellis, C. N., Traverse, C. C., Mayo-Smith, L., Buskirk, S. W., & Cooper, V. S. (2015). Character displacement and the evolution of niche complementarity in a model biofilm community. *Evolution; International Journal of Organic Evolution*, *69*(2), 283–293. https://doi.org/10.1111/evo.12581

Ferguson, G. C., Bertels, F., & Rainey, P. B. (2013). Adaptive Divergence in Experimental Populations of Pseudomonas fluorescens. V. Insight into the Niche Specialist Fuzzy Spreader Compels Revision of the Model Pseudomonas Radiation. *Genetics*, *195*(4), 1319–1335. https://doi.org/10.1534/genetics.113.154948

Flemming, H.-C., & Wuertz, S. (2019). Bacteria and archaea on Earth and their abundance in biofilms. *Nature Reviews Microbiology*, *17*(4), 247–260. https://doi.org/10.1038/s41579-019-0158-9

Flynn, K. M., Dowell, G., Johnson, T. M., Koestler, B. J., Waters, C. M., & Cooper, V. S. (2016). Evolution of Ecological Diversity in Biofilms of Pseudomonas aeruginosa by Altered

Cyclic Diguanylate Signaling. *Journal of Bacteriology*, *198*(19), 2608–2618. https://doi.org/10.1128/JB.00048-16

Gloag, E. S., Marshall, C. W., Snyder, D., Lewin, G. R., Harris, J. S., Santos-Lopez, A., Chaney, S. B., Whiteley, M., Cooper, V. S., & Wozniak, D. J. (2019). Pseudomonas aeruginosa Interstrain Dynamics and Selection of Hyperbiofilm Mutants during a Chronic Infection. *mBio*, *10*(4), e01698-19. https://doi.org/10.1128/mBio.01698-19

Ha, D.-G., Richman, M. E., & O'Toole, G. A. (2014). Deletion Mutant Library for Investigation of Functional Outputs of Cyclic Diguanylate Metabolism in Pseudomonas aeruginosa PA14. *Applied and Environmental Microbiology*, *80*(11), 3384–3393. https://doi.org/10.1128/AEM.00299-14

Habets, M. G. J. L., Rozen, D. E., Hoekstra, R. F., & de Visser, J. A. G. M. (2006). The effect of population structure on the adaptive radiation of microbial populations evolving in spatially structured environments. *Ecology Letters*, *9*(9), 1041–1048. https://doi.org/10.1111/j.1461-0248.2006.00955.x

Hall-Stoodley, L., Costerton, J. W., & Stoodley, P. (2004). Bacterial biofilms: From the Natural environment to infectious diseases. *Nature Reviews Microbiology*, *2*(2), 95–108. https://doi.org/10.1038/nrmicro821

Harris, K. B., Flynn, K. M., & Cooper, V. S. (2021). Polygenic Adaptation and Clonal Interference Enable Sustained Diversity in Experimental Pseudomonas aeruginosa Populations. *Molecular Biology and Evolution*, msab248. https://doi.org/10.1093/molbev/msab248

Hartmann, R., Jeckel, H., Jelli, E., Singh, P. K., Vaidya, S., Bayer, M., Rode, D. K. H., Vidakovic, L., Díaz-Pascual, F., Fong, J. C. N., Dragoš, A., Lamprecht, O., Thöming, J.

G., Netter, N., Häussler, S., Nadell, C. D., Sourjik, V., Kovács, Á. T., Yildiz, F. H., & Drescher, K. (2021). Quantitative image analysis of microbial communities with BiofilmQ. *Nature Microbiology*, *6*(2), 151–156. https://doi.org/10.1038/s41564-020-00817-4

Henriksen, N. N. S. E., Hansen, M. F., Kiesewalter, H. T., Russel, J., Nesme, J., Foster, K. R., Svensson, B., Øregaard, G., Herschend, J., & Burmølle, M. (2022). Biofilm cultivation facilitates coexistence and adaptive evolution in an industrial bacterial community. *Npj Biofilms and Microbiomes*, *8*(1), 1–8. https://doi.org/10.1038/s41522-022-00323-x

Hiniker, A., & Bardwell, J. C. A. (2004). In Vivo Substrate Specificity of Periplasmic Disulfide Oxidoreductases *. *Journal of Biological Chemistry*, *279*(13), 12967–12973. https://doi.org/10.1074/jbc.M311391200

Jenal, U., Reinders, A., & Lori, C. (2017). Cyclic di-GMP: Second messenger extraordinaire. *Nature Reviews Microbiology*, *15*(5), 271–284. https://doi.org/10.1038/nrmicro.2016.190

Kassen, R., & Rainey, P. B. (2004). The Ecology and Genetics of Microbial Diversity. *Annual Review of Microbiology*, *58*(Volume 58, 2004), 207–231. https://doi.org/10.1146/annurev.micro.58.030603.123654

Kessler, C., & Kim, W. (2022). Identification of Cyclic-di-GMP-Modulating Protein Residues by Bidirectionally Evolving a Social Behavior in Pseudomonas fluorescens. *mSystems*, *7*(5), e00737-22. https://doi.org/10.1128/msystems.00737-22

Kessler, C., Mhatre, E., Cooper, V., & Kim, W. (2021). Evolutionary Divergence of the Wsp Signal Transduction Systems in Beta- and Gammaproteobacteria. *Applied and Environmental Microbiology*. https://doi.org/10.1128/AEM.01306-21

Koza, A., Kuśmierska, A., McLaughlin, K., Moshynets, O., & Spiers, A. J. (2017). Adaptive radiation of Pseudomonas fluorescens SBW25 in experimental microcosms provides an understanding of the evolutionary ecology and molecular biology of A-L interface biofilm

1012 formation. *FEMS Microbiology Letters*, *364*(12), fnx109.
1013 https://doi.org/10.1093/femsle/fnx109
1014 Lam, J. S., Taylor, V. L., Islam, S. T., Hao, Y., & Kocíncová, D. (2011). Genetic and Functional
1015 Diversity of Pseudomonas aeruginosa Lipopolysaccharide. *Frontiers in Microbiology*, *2*.
1016 https://doi.org/10.3389/fmicb.2011.00118
1017 Lau, P. C. Y., Lindhout, T., Beveridge, T. J., Dutcher, J. R., & Lam, J. S. (2009). Differential
1018 Lipopolysaccharide Core Capping Leads to Quantitative and Correlated Modifications of
1019 Mechanical and Structural Properties in Pseudomonas aeruginosa Biofilms. *Journal of*
1020 *Bacteriology*, *191*(21), 6618–6631. https://doi.org/10.1128/jb.00698-09
1021 Laventie, Benoit-Joseph, J., Urs. (2020). Surface Sensing and Adaptation in Bacteria. *Annual*
1022 *Review of Microbiology*, *74*(1), 735–760.
1023 Lerouge, I., & Vanderleyden, J. (2002). O-antigen structural variation: Mechanisms and possible
1024 roles in animal/plant–microbe interactions. *FEMS Microbiology Reviews*, *26*(1), 17–47.
1025 https://doi.org/10.1111/j.1574-6976.2002.tb00597.x
1026 Levins, R. (1963). Theory of Fitness in a Heterogeneous Environment. II. Developmental
1027 Flexibility and Niche Selection. *The American Naturalist*, *97*(893), 75–90.
1028 https://doi.org/10.1086/282258
1029 Li, S., Li, T., Teng, X., Lou, X., Xu, Y., Zhang, Q., & Bartlam, M. (2018). Structural analysis of
1030 activating mutants of YfiB from Pseudomonas aeruginosa PAO1. *Biochemical and*
1031 *Biophysical Research Communications*, *506*(4), 997–1003.
1032 https://doi.org/10.1016/j.bbrc.2018.10.190
1033 Malone, J. G., Jaeger, T., Manfredi, P., Dötsch, A., Blanka, A., Bos, R., Cornelis, G. R.,
1034 Häussler, S., & Jenal, U. (2012). The YfiBNR Signal Transduction Mechanism Reveals
1035 Novel Targets for the Evolution of Persistent Pseudomonas aeruginosa in Cystic

1036 Fibrosis Airways. *PLOS Pathogens*, *8*(6), e1002760.
1037 https://doi.org/10.1371/journal.ppat.1002760
1038 Malone, J. G., Jaeger, T., Spangler, C., Ritz, D., Spang, A., Arrieumerlou, C., Kaever, V.,
1039 Landmann, R., & Jenal, U. (2010). YfiBNR Mediates Cyclic di-GMP Dependent Small
1040 Colony Variant Formation and Persistence in Pseudomonas aeruginosa. *PLOS*
1041 *Pathogens*, *6*(3), e1000804. https://doi.org/10.1371/journal.ppat.1000804
1042 Malone, J. G., Williams, R., Christen, M., Jenal, U., Spiers, A. J., & Rainey, P. B. 2007. (2007).
1043 The structure–function relationship of WspR, a Pseudomonas fluorescens response
1044 regulator with a GGDEF output domain. *Microbiology*, *153*(4), 980–994.
1045 https://doi.org/10.1099/mic.0.2006/002824-0
1046 Manta, B., Boyd, D., & Berkmen, M. (2019). Disulfide Bond Formation in the Periplasm of
1047 Escherichia coli. *EcoSal Plus*, *8*(2). https://doi.org/10.1128/ecosalplus.ESP-0012-2018
1048 Martin, M., Hölscher, T., Dragoš, A., Cooper, V. S., & Kovács, Á. T. (2016). Laboratory
1049 Evolution of Microbial Interactions in Bacterial Biofilms. *Journal of Bacteriology*, *198*(19),
1050 2564–2571. https://doi.org/10.1128/jb.01018-15
1051 Marvig, R. L., Sommer, L. M., Molin, S., & Johansen, H. K. (2015). Convergent evolution and
1052 adaptation of Pseudomonas aeruginosa within patients with cystic fibrosis. *Nature*
1053 *Genetics*, *47*(1), 57–64. https://doi.org/10.1038/ng.3148
1054 McDonald, M. J., Gehrig, S. M., Meintjes, P. L., Zhang, X.-X., & Rainey, P. B. (2009). Adaptive
1055 Divergence in Experimental Populations of Pseudomonas fluorescens. IV. Genetic
1056 Constraints Guide Evolutionary Trajectories in a Parallel Adaptive Radiation. *Genetics*,
1057 *183*(3), 1041–1053. https://doi.org/10.1534/genetics.109.107110
1058 McFarland, A. G., Bertucci, H. K., Littman, E., Shen, J., Huttenhower, C., & Hartmann, E. M.
1059 (2021). Triclosan Tolerance Is Driven by a Conserved Mechanism in Diverse

Pseudomonas Species. *Applied and Environmental Microbiology*. https://doi.org/10.1128/AEM.02924-20

Mhatre, E., Snyder, D. J., Sileo, E., Turner, C. B., Buskirk, S. W., Fernandez, N. L., Neiditch, M. B., Waters, C. M., & Cooper, V. S. (2020). One gene, multiple ecological strategies: A biofilm regulator is a capacitor for sustainable diversity. *Proceedings of the National Academy of Sciences*, *117*(35), 21647–21657. https://doi.org/10.1073/pnas.2008540117

Nadell, C. D., Drescher, K., & Foster, K. R. (2016). Spatial structure, cooperation and competition in biofilms. *Nature Reviews Microbiology*, *14*(9), 589–600. https://doi.org/10.1038/nrmicro.2016.84

Oakley, J. L., Weiser, R., Powell, L. C., Forton, J., Mahenthiralingam, E., Rye, P. D., Hill, K. E., Thomas, D. W., & Pritchard, M. F. (2021). Phenotypic and Genotypic Adaptations in Pseudomonas aeruginosa Biofilms following Long-Term Exposure to an Alginate Oligomer Therapy. *mSphere*, *6*(1), 10.1128/msphere.01216-20. https://doi.org/10.1128/msphere.01216-20

O'Connor, J. R., Kuwada, N. J., Huangyutitham, V., Wiggins, P. A., & Harwood, C. S. (2012). Surface sensing and lateral subcellular localization of WspA, the receptor in a chemosensory-like system leading to c-di-GMP production. *Molecular Microbiology*, *86*(3), 720–729. https://doi.org/10.1111/mmi.12013

O'Neal, L., Baraquet, C., Suo, Z., Dreifus, J. E., Peng, Y., Raivio, T. L., Wozniak, D. J., Harwood, C. S., & Parsek, M. R. (2022). The Wsp system of Pseudomonas aeruginosa links surface sensing and cell envelope stress. *Proceedings of the National Academy of Sciences*, *119*(18), e2117633119. https://doi.org/10.1073/pnas.2117633119

O'Rourke, D., FitzGerald, C. E., Traverse, C. C., & Cooper, V. S. (2015). There and back again: Consequences of biofilm specialization under selection for dispersal. *Frontiers in Genetics*, *6*, 18. https://doi.org/10.3389/fgene.2015.00018

O'Toole, G. A., & Kolter, R. (1998). Initiation of biofilm formation in Pseudomonas fluorescens WCS365 proceeds via multiple, convergent signalling pathways: A genetic analysis. *Molecular Microbiology*, *28*(3), 449–461. https://doi.org/10.1046/j.1365-2958.1998.00797.x

Phippen, C. W., Mikolajek, H., Schlaefli, H. G., Keevil, C. W., Webb, J. S., & Tews, I. (2014). Formation and dimerization of the phosphodiesterase active site of the Pseudomonas aeruginosa MorA, a bi-functional c-di-GMP regulator. *FEBS Letters*, *588*(24), 4631–4636. https://doi.org/10.1016/j.febslet.2014.11.002

Poltak, S. R., & Cooper, V. S. (2011). Ecological succession in long-term experimentally evolved biofilms produces synergistic communities. *The ISME Journal*, *5*(3), 369–378. https://doi.org/10.1038/ismej.2010.136

Quigley, C. F., Zhao, Z., Cho, N., Matela, A., Siatkowski, C., Thiagarajan, S., & Cooper, V. (2025, January). *EvolvingSTEM: Exploring Authentic Research Experiences Effects on STEM Occupational Identity Development for Grades 6-12*. The Association for Science Teacher Education (ASTE) Meeting, Long Beach, CA.

Rainey, P. B., & Travisano, M. (1998). Adaptive radiation in a heterogeneous environment. *Nature*, *394*(6688), 69–72. https://doi.org/10.1038/27900

Røder, H. L., Sørensen, S. J., & Burmølle, M. (2016). Studying Bacterial Multispecies Biofilms: Where to Start? *Trends in Microbiology*, *24*(6), 503–513. https://doi.org/10.1016/j.tim.2016.02.019

1105 Rybtke, M. T., Borlee, B. R., Murakami, K., Irie, Y., Hentzer, M., Nielsen, T. E., Givskov, M.,
1106 Parsek, M. R., & Tolker-Nielsen, T. (2012). Fluorescence-based reporter for gauging
1107 cyclic di-GMP levels in Pseudomonas aeruginosa. *Applied and Environmental*
1108 *Microbiology*, *78*(15), 5060–5069. https://doi.org/10.1128/AEM.00414-12
1109 Santos-Lopez, A., Marshall, C. W., Scribner, M. R., Snyder, D. J., & Cooper, V. S. (2019).
1110 Evolutionary pathways to antibiotic resistance are dependent upon environmental
1111 structure and bacterial lifestyle. *eLife*, *8*, e47612. https://doi.org/10.7554/eLife.47612
1112 Schindelin, J., Arganda-Carreras, I., Frise, E., Kaynig, V., Longair, M., Pietzsch, T., Preibisch,
1113 S., Rueden, C., Saalfeld, S., Schmid, B., Tinevez, J.-Y., White, D. J., Hartenstein, V.,
1114 Eliceiri, K., Tomancak, P., & Cardona, A. (2012). Fiji: An open-source platform for
1115 biological-image analysis. *Nature Methods*, *9*(7), 676–682.
1116 https://doi.org/10.1038/nmeth.2019
1117 Schweizer, H. P. (2001). Triclosan: A widely used biocide and its link to antibiotics. *FEMS*
1118 *Microbiology Letters*, *202*(1), 1–7. https://doi.org/10.1111/j.1574-6968.2001.tb10772.x
1119 Scribner, M. R., Santos-Lopez, A., Marshall, C. W., Deitrick, C., & Cooper, V. S. (2020). Parallel
1120 Evolution of Tobramycin Resistance across Species and Environments. *mBio*, *11*(3),
1121 e00932-20. https://doi.org/10.1128/mBio.00932-20
1122 Smith, E. E., Buckley, D. G., Wu, Z., Saenphimmachak, C., Hoffman, L. R., D'Argenio, D. A.,
1123 Miller, S. I., Ramsey, B. W., Speert, D. P., Moskowitz, S. M., Burns, J. L., Kaul, R., &
1124 Olson, M. V. (2006). Genetic adaptation by Pseudomonas aeruginosa to the airways of
1125 cystic fibrosis patients. *Proceedings of the National Academy of Sciences*, *103*(22),
1126 8487–8492. https://doi.org/10.1073/pnas.0602138103
1127 Spiers, A. J. (2014). Getting Wrinkly Spreaders to demonstrate evolution in schools. *Trends in*
1128 *Microbiology*, *22*(6), 301–303. https://doi.org/10.1016/j.tim.2014.03.007

Spiers, A. J., Bohannon, J., Gehrig, S. M., & Rainey, P. B. (2003). Biofilm formation at the air–liquid interface by the Pseudomonas fluorescens SBW25 wrinkly spreader requires an acetylated form of cellulose. *Molecular Microbiology*, *50*(1), 15–27. https://doi.org/10.1046/j.1365-2958.2003.03670.x

Spiers, A. J., Kahn, S. G., Bohannon, J., Travisano, M., & Rainey, P. B. (2002). Adaptive Divergence in Experimental Populations of Pseudomonas fluorescens. I. Genetic and Phenotypic Bases of Wrinkly Spreader Fitness. *Genetics*, *161*(1), 33–46. https://doi.org/10.1093/genetics/161.1.33

States, N. L. (2013). *Next Generation Science Standards: For States, By States*. National Academies Press.

Stewart, P. S., & Franklin, M. J. (2008). Physiological heterogeneity in biofilms. *Nature Reviews Microbiology*, *6*(3), 199–210. https://doi.org/10.1038/nrmicro1838

Taylor, M. B., Warwick, A. R., Skophammer, R., Boyer, J. M., Geck, R. C., Gunkelman, K., Walson, M., Rowley, P. A., & Dunham, M. J. (2024). yEvo: A modular eukaryotic genetics and evolution research experience for high school students. *Ecology and Evolution*, *14*(1), e10811. https://doi.org/10.1002/ece3.10811

Trampari, E., Holden, E. R., Wickham, G. J., Ravi, A., Martins, L. de O., Savva, G. M., & Webber, M. A. (2021). Exposure of Salmonella biofilms to antibiotic concentrations rapidly selects resistance with collateral tradeoffs. *Npj Biofilms and Microbiomes*, *7*(1), 1–13. https://doi.org/10.1038/s41522-020-00178-0

Traverse, C. C., Mayo-Smith, L. M., Poltak, S. R., & Cooper, V. S. (2013). Tangled bank of experimentally evolved Burkholderia biofilms reflects selection during chronic infections. *Proceedings of the National Academy of Sciences*, *110*(3), E250–E259. https://doi.org/10.1073/pnas.1207025110

Trubenová, B., Roizman, D., Moter, A., Rolff, J., & Regoes, R. R. (2022). Population genetics, biofilm recalcitrance, and antibiotic resistance evolution. *Trends in Microbiology*, *30*(9), 841–852. https://doi.org/10.1016/j.tim.2022.02.005

Turner, C. B., Marshall, C. W., & Cooper, V. S. (2018). Parallel genetic adaptation across environments differing in mode of growth or resource availability. *Evolution Letters*, *2*(4), 355–367. https://doi.org/10.1002/evl3.75

Wei, Q., Leclercq, S., Bhasme, P., Xu, A., Zhu, B., Zhang, Y., Zhang, M., Wang, S., & Ma, L. Z. (2019). Diguanylate Cyclases and Phosphodiesterases Required for Basal-Level c-di-GMP in Pseudomonas aeruginosa as Revealed by Systematic Phylogenetic and Transcriptomic Analyses. *Applied and Environmental Microbiology*, *85*(21), e01194-19. https://doi.org/10.1128/AEM.01194-19

Xu, A., Wang, D., Wang, Y., Zhang, L., Xie, Z., Cui, Y., Bhamse, P., Yu, H., Zhang, X.-X., Li, D., & Ma, L. Z. (2021). Mutations in surface-sensing receptor WspA lock the Wsp signal transduction system into a constitutively active state. *Environmental Microbiology*, *n/a*(n/a). https://doi.org/10.1111/1462-2920.15763

Xu, M., Yang, X., Yang, X.-A., Zhou, L., Liu, T.-Z., Fan, Z., & Jiang, T. (2016). Structural insights into the regulatory mechanism of the Pseudomonas aeruginosa YfiBNR system. *Protein & Cell*, *7*(6), 403–416. https://doi.org/10.1007/s13238-016-0264-7

Yang, X., Yang, X., Xu, M., Zhou, L., Fan, Z., & Jiang, T. (2015). Crystal structures of YfiR from Pseudomonas aeruginosa in two redox states. *Biochemical and Biophysical Research Communications*, *461*(1), 14–20. https://doi.org/10.1016/j.bbrc.2015.03.160

Yu, L., Cao, Q., Chen, W., Yang, N., Yang, C.-G., Ji, Q., Wu, M., Bae, T., & Lan, L. (2022). A novel copper-sensing two-component system for inducing Dsb gene expression in bacteria. *Science Bulletin*, *67*(2), 198–212. https://doi.org/10.1016/j.scib.2021.03.003

Zhao, K., Tseng, B. S., Beckerman, B., Jin, F., Gibiansky, M. L., Harrison, J. J., Luijten, E., Parsek, M. R., & Wong, G. C. L. (2013). Psl trails guide exploration and microcolony formation in Pseudomonas aeruginosa biofilms. *Nature*, *497*(7449), 388–391. https://doi.org/10.1038/nature12155